# Technical Note on Quality Assessment for SkySat
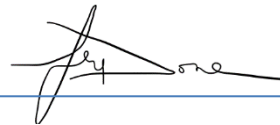
| | | |
|---|---|---|
| Author(s): | | **Sébastien Saunier**<br>**Sultan Kocaman**<br>*Task 1 Mission Expert* |
| Approval: | | ***Fay Done***<br>*Task 1 Lead* |
| Accepted: | | ***Clement Albinet***<br>*ESA Technical Officer* |

# AMENDMENT RECORD SHEET

The Amendment Record Sheet below records the history and issue status of this document.

| ISSUE | DATE | REASON |
|:---:|:---:|:---|
| 0.1 | 26 02 2020 | Draft version for ESA review |
| 0.2 | 03 03 2020 | Draft version for ESA review – updated maturity matrix (Table 2-1) to account for not public information |
| 0.3 | 06 07 2021 | Draft version for ESA review. All sections updated. |
| 1.0 | 06 09 2021 | Final version for issue. |

# TABLE OF CONTENTS

# 1. INTRODUCTION

This technical note details the results of the (preliminary) mission data quality assessments (including geometric calibration, radiometric calibration and image quality) performed on a sample of products generated for *SkySat (SKS)*, a constellation of commercial Earth Observation (**EO**) optical satellites operated by Planet.

The aforementioned mission data quality assessments are performed in accordance with the assessment guidelines, detailed in [RD-1, RD-2], that constitute the European Space Agency (**ESA**) Earthnet Data Assessment Pilot (**EDAP**) Project's *EO Mission Data Quality Assessment Framework*. An important representation of the latter framework, constructed by the National Physical Laboratory (**NPL**), is what is known as the *maturity matrix*. It is a diagrammatic summary of the following:

- *Documentation Review: the EDAP Optical team reviews materials (e.g. data and documentation) provided by the data provider or operator, some of which may not be publically available, or even the scientific community (e.g. published papers). The results are detailed in Section 3 (covering the first four columns of the maturity matrix).*

- *Data Quality Assessments: the EDAP Optical team performs data quality assessments (i.e. validation assessments), independently of any validation assessments performed by the data provider and / or operator. The results are detailed in Section 4 (covering the last column, 'Validation', of the maturity matrix).*

The above assessments are performed by the EDAP Optical team using the appropriate in-house and open-source ad-hoc scripts / tools.

It is important to note the purpose of the aforementioned framework is to ensure that the delivered commercial mission data is fit for purpose and that all decisions regarding the inclusion of the commercial mission as an ESA third party mission can be made fairly and with confidence.

## 1.1 Reference Documents

The following is a list of reference documents with a direct bearing on the content of this proposal. Where referenced in the text, these are identified as [RD-n], where 'n' is the number in the list below:

RD-1.   EDAP.REP.001 Generic EDAP Best Practice Guidelines,1.1 23 May 2019

RD-2.   EDAP.REP.002 Optical Mission Quality Assessment Guidelines, 1.0, 16 October 2019.

RD-3.   Planet Imagery Product Specifications, June 2020, https://assets.planet.com/docs/Planet_Combined_Imagery_Product_Specs_letter_screen.pdf

RD-4.   Analysis Ready Data for Land, product family specification Surface Reflectance (CARD-4L SR), 08/06/2020 http://ceos.org/ard/files/PFS/SR/v5.0/CARD4L_Product_Family_Specification_Surface_Reflectance-v5.0.pdf

RD-5.   Planet L1 Data Quality Report Q3 2020 – Status of calibration and Data Quality for the SKS Constellation

RD-6.   Leachtenauer, J. et al, 1997. General Image-Quality Equation: GIQE. Applied Optics, Vol. 36, No. 32, pp. 8322 – 8328.

RD-7.   Valenzuela, A. Q. and J. C. G. Reyes. "Comparative Study of the different versions of the General Image Quality Equation." ISPRS Annals of the Photogrammetry, Remote Sensing and Spatial Information Sciences (2019): 493-500.

RD-8.   NEXTMap World 30 Digital Surface Model, Intermap (083013v3)

RD-9.   Andrea's Burn, "SKS Initial Radiometric Correction and Radiometric Calibration", JACIE conference, 2018

RD-10. Adrian Gonzalez, "Absolute Calibration and Validation of SKS Constellation", VH Roda                                    conference,                                    2019 https://earth.esa.int/documents/700255/4038567/3+VH+Roda+-+ESA+Rome+Nov.+2019+-+Adrian+Gonzalez.pdf

RD-11. Biron Smiley, "Long Term Geometric Stability of the SKS Constellation" Processing of JACIE Conference, September, 19 2018

RD-12. Zanoni, "IKONOS Signal-to-Noise Ratio Estimation", March 25-27, 2002, JACIE Workshop, 2002 https://ntrs.nasa.gov/search.jsp?R=20040004380

RD-13. P. Blanc, "Image Quality – WP224", TN-WP224-001-ARMINES, September 26, 2018

RD-14. Françoise Viallefont-Robinet, Dennis Helder, Renaud Fraisse, Amy Newbury, Frans van den Bergh, Donghan Lee, Sébastien Saunier.. Comparison of MTF measurements using edge method: towards reference data set. Optics Express, Optical Society of America, 2018, 26 (26), pp.33625-33648. ⟨hal-02055611⟩

RD-15. S. Saunier, P. Goryl, G. Chander, M. Bouvet, R. Santer and S. Kocaman, "Radiometric, geometric and image quality assessment of the ALOS AVNIR-2 and PRISM sensors," TGRS, 48(10), 3855-3866 (2010).
RD-16. K. Kohm, "Modulation transfer function measurement method and results for the Orbview-3 high resolution imaging satellite," Proceedings of ISPRS, Istanbul, Turkey (2004).

RD-17. H. Cosnefroy, M. Leroy, X. Briottet, Selection and characterization of Saharan and Arabian desert sites for the calibration of optical satellite sensors, Remote Sensing of Environ.,        Vol.        58,        N°1,        pp        101-114,        1996 https://www.sciencedirect.com/science/article/abs/pii/0034425795002111?via%3Dihub

RD-18. Saunier, Sébastien & Goryl, Philippe & Chander, Gyanesh & Santer, Richard & Bouvet, Marc & Collet, Bernard & Mambimba, Aboubakar & Kocaman, Sultan. (2010). Radiometric, geometric, and image quality assessment of ALOS AVNIR-2 and PRISM sensors.   IEEE   T.   Geoscience   and   Remote   Sensing.   48. 10.1109/TGRS.2010.2048714. https://www.researchgate.net/publication/262804365_Radiometric_geometric_and_image_quality_assessment_of_ALOS_AVNIR-2_and_PRISM_sensors

RD-19. M. Bouvet, "Intercomparison of multispectral imagers over natural targets," in Proc. IGARSS, Barcelona, Spain, 2007 https://doi.org/10.1109/IGARSS.2007.4423390

RD-20. H. Murakami, T. Tadono, H. Imai, J. Nieke, and M. Shimada, "Improvement of AVNIR-2 Radiometric Calibration by Comparison of Cross-Calibration and Onboard Lamp Calibration," IEEE Trans. Geoscience and Remote Sensing, vol. 47, no. 12, pp. 4051–4059,                        Dec.                        2009 https://www.researchgate.net/deref/http%3A%2F%2Fdx.doi.org%2F10.1109%2FTGRS.2009.2018118

RD-21. G. Chander, D. Meyer, and D. L. Helder, "Cross-calibration of the Landsat 7 ETM+ and EO ALI sensor," IEEE Transactions on Geoscience and Remote Sensing, vol. 42, no. 12, pp. 2821–2831, Dec. 2004 https://ieeexplore.ieee.org/document/1369378

RD-22. K. J. Thome, "In-flight intersensor radiometric calibration using vicarious approaches," Post-Launch Calibration of Satellite Sensors, Edited by S. A. Morain and A. M. Budge, Balkema Publishers, Philadephia, pp. 93-102, 2004 https://www.researchgate.net/publication/260182735_Inflight_Intersensor_Radiometric_Calibration_using_the_Reflectance-Based_Method_for_Landsat-Type_Sensors

RD-23. Biron Smiley, "Long Term Geometric Stability of the SKS Constellation" Processing of JACIE Conference, September, 19 2018

RD-24. Aati S, Avouac J-P. Optimization of Optical Image Geometric Modeling, Application to Topography Extraction and Topographic Change Measurements Using PlanetScope and SKS Imagery. Remote Sensing. 2020; 12(20):3418. https://doi.org/10.3390/rs12203418

RD-25. Murthy, K., Shearn, M., Smiley, B. D., Chau, A. H., Levine, J., & Robinson, M. D. (2014, October). SKS-1: very high-resolution imagery from a small satellite. In Sensors, Systems, and Next-Generation Satellites XVIII (Vol. 9241, p. 92411E). International Society for Optics and Photonics.

RD-26. Bhushan, S., Shean, D., Alexandrov, O., & Henderson, S. (2021). Automated digital elevation model (DEM) generation from very-high-resolution Planet SKS triplet stereo and video imagery. ISPRS Journal of Photogrammetry and Remote Sensing, 173, 151-165.

RD-27. d'Angelo, P., Kuschk, G., & Reinartz, P. (2014). Evaluation of skybox video and still image products. The International Archives of the Photogrammetry, Remote Sensing and Spatial Information Sciences, Volume XL-1, 2014, ISPRS Technical Commission I Symposium, 17 – 20 November 2014, Denver, Colorado, USA.

RD-28. Anger, J., Ehret, T., & Facciolo, G. (2021). Parallax estimation for push-frame satellite imagery: application to super-resolution and 3D surface modeling from SKS products. arXiv preprint arXiv:2102.02301.

RD-29. ESA Copernicus (2021). SKS. https://spacedata.copernicus.eu/fr/SKS (accessed on 11 Mar 2021)

## 1.2 Glossary

The following acronyms and abbreviations have been used in this report.

| | |
|---|---|
| ATBD | Algorithm Theoretical Baseline Document |
| AC | ACross-track |
| AL | ALong-track |
| BOA | Bottom of Atmosphere |
| BRDF | Bidirectional Reflectance Distribution Function |
| CCD | Charge-Coupled Device |
| CEOS | Committee on Earth Observation Satellites |

| EDAP | EarthNet Data Assessment Pilot |
|------|-------------------------------|
| ESF | Edge Spread Function |
| FWHM | Full Width at Half Maximum |
| GCP | Ground Control Points |
| HR | High Resolution |
| IFOV | Instantaneous Field of View |
| JACIE | Joint Agency Commercial Imagery Evaluation |
| LSF | Line Spread Function |
| MTF | Modulation Transfer Function |
| NPL | National Physical Laboratory |
| PDI | Product Data Item |
| PICS | Pseudo-invariant Calibration Site |
| PBHDR | Push-broom High Dynamic Range |
| RMSE | Root Mean Square Error |
| SNR | Signal-to-Noise Ratio |
| SKS | SkySat |
| TN | Technical Note |
| TOA | Top-Of-Atmosphere |
| UDM2 | Usable Data Mask |
| UDM | Unusable Data Mask |
| VHR | Very High Resolution |

## 2.    EDAP MATURITY MATRIX

The EDAP data quality assessments relied, firstly, on documentation disclosed by the data provider ([RD-3, RD-5]). This documentation included information on product format, product processing, data validation, as well as more specific / technical documentation and existing publications (conference proceedings, peer-reviewed papers) ([RD-9 - RD-11]).

The EDAP data quality assessments (i.e. EDAP validation), detailed in Section 4, have been focused on a sample of SKS Basic Scene (Level 1A) and Ortho Scene (Level 1C) products from SKS 1, 4, 7, 10, 12, in the Summer and Autumn of 2020. These products were generated in the last quarter of 2020 and the first quarter of 2021.

The results of the EDAP data quality assessments are captured within the maturity matrix, given in Table 2-1, where a summary for each section of it is detailed below.

### Product Information

The mission, products and product format are well documented and the data easily accessible. However, a detailed description of processing algorithms used is not shared, the product format does not include information on the measurement data quality and there is no traceability chain documented.

### Product Generation

The processing steps undertaken to produce the data are documented from the user point of view with very limited details on the processing itself. Unfortunately, EDAP has not been able to access to any documents on pre-flight activities. On the other hand, regarding the in-flight calibration activities, there are a few documents that show that Planet is using appropriate community infrastructure to undertake these activities. These documents should be updated more regularly.

### Ancillary Information

The Planet product includes some useful ancillary information, including product flags (mostly binary (unusable mask data, set per pixel)). The product includes little information in general and the format (JSON) is not designed to include information on ancillary data origin, ancillary data type, uncertainties, etc. The Planet team have shared some valuable ancillary information, not included in the product, such as the relative spectral responses.

### Uncertainty Characterisation

The quarterly Planet data quality report ([RD-5]) provides evidence that the quality of the mission products is regularly monitored. The quarterly report details a comprehensive assessment of the most common product performance quality items. There is some room for improvements regarding uncertainty sources because they are, except for the geometry, not discussed. Moreover, quarterly report gives high priority to document image quality artefacts such as parallax effects, over-sharpening, data saturation and processing chain issues.

### Validation

- Image Quality
  - Visual Inspection: In general, the imagery does not show evidence of image artefacts or anomalies that are detectable through visual inspection (except for some, within specific image regions, already observed and documented by Planet). Unfortunately, through visual inspection, it has also been determined that the image quality differs strongly depending on the satellite involved in the observation and capture settings used.

- o Signal-to-Noise Ratio: By using bright uniform site, it has been possible to compute the Signal-to-Noise Ratio (**SNR**) for a full image. The assessment results indicate the SNR is stable and compliant with the Planet specification
- o Modulation Transfer Function: By using the artificial Modulation Transfer Function (**MTF**) target located in La Crau, the spatial resolution of SKS 0.5 m data has been estimated.
- Geometric Calibration Validation: The geometric accuracy is validated under the categories of absolute, relative (temporal), interband and stereoscopic capability. The results are within the specifications provided by Planet (see [RD-3]).
- Radiometric Calibration Validation: The radiometric accuracy assessment is based on an absolute calibration methodology applied on the Committee on Earth Observation Satellite (**CEOS**) Pseudo Invariant Calibration Site (**PICS**) data. The results are heterogeneous but remain within the specifications provided by Planet (see [RD-3]).

**Table 2-1: SKS Quality Maturity Matrix**

| Product Information | Product Generation | Ancillary Information | Uncertainty Characterisation | Validation |
|---|---|---|---|---|
| Product Details | Sensor Calibration & Characterisation Pre-Flight | Product Flags | Uncertainty Characterisation Method 🔒 | Reference Data Representativeness |
| Product Availability & Accessibility | Sensor Calibration & Characterisation Post-Launch 🔒 | Ancillary Data | Uncertainty Sources Included 🔒 | Reference Data Quality |
| Product Format | Retrieval Algorithm Method | | Uncertainty Values Provided 🔒 | Validation Method |
| User Documentation | Retrieval Algorithm Tuning | | Geolocation Uncertainty 🔒 | Validation Results |
| Metrological Traceability Documentation | Additional Processing | | | |

| Key |
|---|
| Not Assessed |
| Not Assessable |
| Basic |
| Intermediate |
| Good |
| Excellent |

🔒 Information not public

# 3. DETAILED EDAP QUALITY ASSESSMENT

## 3.1 Product Information

This section covers a review of top-level product description information, product format, and the supporting documentation. The table below details general product information for SKS (note the values of some of these parameters can be found in any product, written within the JSON file, but the rest can be found in the available user documentation).

| Product Details | |
|---|---|
| **Product Name** | *Basic Scene Product (Level 1A)*<br>*Ortho Scene Product (Level 1C)*<br>*Ortho Collect (Level 1C_C: Ortho Collect Product, including up to 60 scenes, (20 per camera)* |
| **Sensor Name** | *SKS* |
| **Sensor Type** | *CMOS Frame Camera (Multi-Spectral and Panchromatic)* |
| **Mission Type** | *Satellite Constellation* |
| **Mission Orbit** | *Low Earth Sun Synchronous Orbit* |
| **Product Version Number** | *The product version number of the product is not tagged in the product format.* |
| **Processor Name / Version** | *The processor name or version that generated the product is not tagged in the product format.* |
| **Product ID** | *<AcquisitionDate>_<AcquisitionTime>_<SatelliteID><CameraID>_<FrameId>*<br>*Example: 20200718_082806_ssc4d1_0008* |
| **Processing level of product** | *Level 1A and Level 1C ( Ortho Scene, Ortho Collect )*<br>*(Level 1C_C: Ortho Collect Product, including up to 60 scenes, (20 per camera)* |
| **Measured Quantity Name** | *Digital number to Radiance (SI)* and *Top of Atmosphere Reflectance (SI)* |
| **Measured Quantity Units** | *Not available in the metadata*<br>*(DN / W sr$^{-1}$ m$^{-2}$ $\mu$m$^{-1}$ )* |
| **Stated Measurement Quality** | *Unavailable* |
| ***Spatial Resolution*** | *The ground sampling distance (GSD) depends on the satellite altitude. Whatever the sensor band (Multispectral, Panchromatic), the GSD is within 0.6 m and 0.95 m.* |

| | |
|---|---|
| | *There is an upscaling of the data, and the pixel size of the ortho scene product images (Multi spectral and Panchromatic) is 0.5 m. Moreover, pansharpened products (0.5 m pixel spacing) are also proposed to the customer.* |
| **Spatial Coverage** | *The spatial coverage is given in the JSON file with the geographical coordinates of the product footprint (corners). (For information, the image size of one basic scene (one camera) is about 250 pixels x 1080 pixels (image width / image height), applicable for multispectral and panchromatic data.)* |
| **Temporal Resolution** | *The temporal resolution is not indicated as metadata information. The temporal resolution should not exceed one day accounting for the overall information.* |
| **Temporal Coverage** | *The temporal coverage understood as the scene time duration is not indicated in the product metadata.* |

There is a minimum set of information available in the product format but relevant information is mostly available in the user guide [RD-3]. In the product format, there is no information on the measurement data quality. Furthermore, any required and recommended information, including point of contact and product locator, is missing. For these reasons, the EDAP grade of **Product Details** is "*Basic*".

The data set meets many of the *Findable, Accessible, Interoperable and Reusable (FAIR) Principles* but there is no data management plan. For this reason, the EDAP grade of **Product Availability and Accessibility** is '*intermediate'*.

The data product includes encoded GeoTiff images with GeoJSON metadata file. The data product format is well documented [RD-3] and meets scientific community naming conventions / standards. The compliancy to CARD4L-Sxfurequirements is not reached because processing algorithms and auxiliary data are not identified in the metadata. For these reasons, the EDAP grade for data **Product Format** is *'Good'.*

The user documentation covers two fundamental aspects, a product user guide and an Algorithm Theoretical Basis Document (**ATBD**); the Planet user guide [RD-3], which is very detailed, contains ATBD-type information (in the absence of a formal ATBD). In addition to the latter, user documentation in the form of conference presentations are accessible online. For these reasons, the EDAP grade for **User Documentation** is *'Intermediate'.*

The metrological traceability chain has not been documented and so for this reason the EDAP grade for **Metrological Traceability Documentation** is *'Not Assessable'.*

## 3.2    Product Generation

The product generation section covers the processing steps undertaken to produce the data, including the calibration algorithm, retrieval algorithm and additional processing. As mentioned previously, the data provider delivers Level 1A and Level 1C data products.

Regarding the pre-flight calibration and characterisation activities, the EDAP team did not find relevant documentation and so for this reason the EDAP grade for **Sensor Calibration and Characterisation Pre-Flight** is *'Not Assessable'.*

The post-launch calibration and characterisation activities are well documented as discussed in [RD-9], [RD-10], [RD-11]; the Planet calibration / validation team has focused on important aspects of sensor behaviour and are reliant, as much as possible, on community infrastructure for their activities. For these reasons, the EDAP grade for **Sensor Calibration and Characterisation Post-launch** is *'Intermediate'.*

The data provider does not deliver SKS surface reflectance product derived from the standard Planet Analytic (Radiance). For this reason, the EDAP grade of **Retrieval Algorithm Method** and **Retrieval Algorithm Tuning** is *'Not Assessable'.*

The information on additional processing, which is mainly found in the user guide [RD-3], refers to geometric and pan sharpening processing in this case; for geometric processing, the basic processing stages have been detailed along with the specifications on reference data sources (ground control points (**GCP**s) and Digital Elevation Model (**DEM**)) in [RD-3] and [RD-8]. There is no ATBD-type information on geometric processing, and there is no information on pan-sharpening at all, and for this reason the EDAP grade of **Additional Processing** is '*Basic*'.

## 3.3    Ancillary Information

The data product contains a limited set of well documents Unusable Data Mask (**UDM**) flags that are mostly binary in nature and so for this reason the EDAP grade for **Product Flags** is '*Intermediate'.*

The ancillary data provided is to define measurement, but other information on ancillary data has to be requested through the user service (e.g. relative spectral response function) and so the EDAP grade for **Ancillary Data** is *'Basic'.*

## 3.4    Uncertainty Characterisation

This section of the mission quality assessment evaluates the methodology used to estimate uncertainty values for a given mission, the extent of the mission's assessment and how the values are provided.

The Planet team perform regular uncertainty characterisation activities as illustrated in the quarterly data quality report [RD-5]. The quarterly report is not public but it has been shared with the EDAP team under a non-disclosure agreement.

Based on representative dataset and comparison with other sensors, the quarterly report proposes a comprehensive assessment of the most common product performance quality items. Furthermore, a full breakdown is proposed. For these reasons, the EDAP grade for **Uncertainty Characterisation Method** is *'Good'.*

The uncertainty sources are specifically discussed for the geometric method (raster reference data). There is no similar discussion regarding the other method. For this reason, the EDAP grade for **Uncertainty Sources** is 'Basic'.

The uncertainty values are not provided in the data product. However, the main uncertainty values given in [RD-5] are provided for subsets of data (e.g. sample of data for a given period). For some assessment, per satellite results are provided, as for SNR. In addition, the uncertainty values are in most cases expressed into representative systems (metrics), which are very helpful for the user.

For all of these reasons, EDAP grade for **Uncertainty Values** and **Geolocation Uncertainty** is '*Intermediate*'.

The tables below summarise the uncertainty values gathered from the existing documentation and covering sub set of data observed in the Q3 2020 period. These values have been used

as input of the EDAP quality assessments, as also written at the beginning of each corresponding quality assessment section (when relevant).

| Uncertainty Values Provided: Radiometric Calibration Uncertainty | |
|---|---|
| Summary | *The Planet assessment is performed based on RadCalNet data as reference. The following mean / STD accuracy are given (all satellites, except C14 – C19):*<br>• *Blue : 0.0858 / 0.2677*<br>• *Green : 0.1183 / 0.2642*<br>• *Red: 0.0255 / 0.2294*<br>• *NIR: 0.0833 / 0.2368*<br>*The mean / STD accuracy values are statistics over one sample. One sample includes a set of percent difference (SKS / RadCalNet) results computed at overpass time and for the entire RadCalNet network.*<br>*In the Planet team results, no distinction is made depending on detector and satellite involved. The aforementioned results are not applicable to C14 to C19 satellites, for which radiometric calibration is in progress.*<br>*The mean accuracy is mostly below 10 % and it is perfectly in agreement with claimed specification. However, it is observed the STD is very high and it leads to a degraded uncertainty.*<br><br>*The Planet team acknowledges that the method does not take into account directional effects, it might explain reason for which errors are dispersed around the mean value.*<br>*Note that in [RD-5], the proposed additional precision index (uncertainty at 68 percentile, uncertainty at 95 percentile) does not take into consideration the hypothesis on probability density curve of errors.* |
| Reference | [RD-5] |

| Uncertainty Values Provided: Signal-to-Noise Ratio | |
|---|---|
| Summary | *For SKS, the standard SNR parameter is not provided. Rather, differential SNR metric (gSNR) (refer to [RD-5] for the definition of differential SNR metric) is used and accuracy results are the following one (all satellites together):*<br>• *Blue: 34.498*<br>• *Green: 42.703*<br>• *Red: 45.399*<br>• *NIR: 41.836*<br>• *Pan: 173.605*<br>*The minimal requirements given by data provider are respectively 30, 75 for MS, PAN bands, meaning that results are within requirements.*<br>*The differential SNR is computed on satellite basis and detailed results are given. However, the number of measurements involved is not given.*<br>*The Push-Broom High Dynamic Range (**PBHDR**) imaging mode improves SNR results. Also, depending on the satellite for which this imaging mode is applicable, differential SNR results differs; results are lower when PBHDR is active. Increasing SNR is essential to improve up scaling process; from native GSD up to 0.5 m pixel map spacing.* |

| | |
|---|---|
| | *It is worth noting that providing differential SNR values enables direct insertion within the GIQE equation [RD-6], Mathematical formulation of Planet SNR metric is similar to the Signal Difference to Noise Ratio (SDNR), widely shared in the community* |
| Reference | [RD-5] |

| Uncertainty Values Provided: Relative Edge Response | |
|---|---|
| Summary | *The Relative Edge Response (RER) is calculated for Blue, Green, Red, NIR and Pan bands for any images with sharp edges overlapping 5000 specified airport sites worldwide. The RER is the effective slope of the normalised edge profile. As disclosed by the data provider, the RER results are the following ones:*<br><br>• *Blue: 0.275*<br><br>• *Green: 0.301*<br><br>• *Red: 0.338*<br><br>• *NIR: 0.256*<br><br>• *Pan: 0.303*<br><br>*The RER is a good indicator of image sharpness. The other commonly known image quality parameters, such as Full Width at Half Maximum (FWHM) or Modulation Transfer Function (MTF) value at Nyquist frequency are not shared.* |
| Reference | [RD-5] |

Applicable to all geolocation uncertainty items, Planet proposes an "overall" geolocation uncertainty metrics applicable to the SKS constellation. Also, the following metrics are given:

- Average root-mean-square error (**RMSE**),
- 90th percentile of the radial RMSE,
- Standard deviation (**STD**) of RMSE.

The table below details the geolocation uncertainty results.

| Geolocation Uncertainty | |
|---|---|
| Summary | The product accuracy results (Level 1C), reported by the quality control team and considered as EDAP input specifications, are given in [RD-5]. They can be summarised as follow:<br><br>• *The absolute geolocation accuracy is 3.4 m / 2.6 m (Mean / STD RMSE accuracy), this average accuracy is computed based on 50139 products,*<br><br>• *The temporal geolocation accuracy is 3.1 m / 5.7 m (Mean / STD RMSE accuracy), this average accuracy is computed based on 55496 products.*<br><br>• *The inter-band registration accuracy (Mean / STD RMSE Accuracy) is summarised as follow:*<br><br>    *Blue - Green : 0.11 m / 0.06 m*<br><br>    *Blue - Red   : 0.13 m / 0.08 m*<br><br>    *Blue - NIR   : 0.22 m / 0.14 m*<br><br>    *Green - Red : 0.09 m / 0.05 m*<br><br>    *Green - NIR  : 0.20 m / 0.12 m* |

| | |
|---|---|
| | *Red - NIR     : 0.18 m / 0.12 m* |
| | *This average accuracy is computed based on about 63900 products.* |
| Reference | [RD-5] |

Note that there is no specification regarding expected elevation accuracy when performing stereo matching.

## 3.5 Validation

The below validation items related to activities conducted by the EDAP Team (not Planet).

Reference measurements are assessed to be somewhat representative of the satellite measurements, covering a limited range of satellite measurements. For this reason, the EDAP grade of **Reference Data Representativeness** is '*Basic'.*

| Reference Data Representativeness | |
|---|---|
| Summary | *Good representativeness but the sample of reference data used as input of the EDAP methodology is small.* |
| Reference | *None. Note that this report provides results of such a validation.* |

The reference data used by EDAP comes with a single uncertainty for the entire data set. For this reason, the EDAP grade of **Reference Data Quality** is '*Intermediate'.*

| Reference Data Quality | |
|---|---|
| Summary | *The Sentinel-2 mission is used as reference as the radiometric accuracy of MSI is high and well documented. Considering both satellites and accuracy attached to atmospheric correction, the absolute calibration uncertainties is within 3%.* <br><br> *Regarding the absolute geolocation, the method used as reference a GCP set derived from a GPS test field survey. The uncertainties of the field measurement is within 2-3 cm. The multi-temporal accuracy is also assessed by using the same GCP set.* <br> *The interband accuracy assessment method does not use external reference.* <br> *The stereoscopic capability assessment was performed by comparison of SKS-generated DSM with UAV-DSM. The UAV-DSM has a global uncertainty value of approximately 5 cm.* |
| Reference | *https://sentinel.esa.int/documents/247904/685211/Sentinel-2_User_Handbook* <br> *https://www.usgs.gov/land-resources/nli/landsat/landsat-8-data-users-handbook* |

The EDAP methodology assess satellite measurements providing a simple uncertainty estimated (e.g. from statistical point of view). For this reason, the EDAP grade of **Validation Method** is '*Intermediate*'.

| Validation Method | |
|---|---|
| Summary | *Absolute geolocation accuracy is validated with GCP set located in the image space by using a semi-automatic method. The uncertainty related to the GCP pointing accuracy is within ½ pixel.* |

| | |
|---|---|
| | *The image matching techniques involved in image grid comparison is very accurate with an uncertainty of about 0.1 pixel.* |
| | *The stereoscopic capability assessment method is based on surface matching and comparison, and has an uncertainty value equal to the reference DSM used in the evaluation (ca. one grid spacing unit).* |
| | *The atmospheric validation is using 6SV and atmospheric values from the Copernicus Atmosphere Monitoring Service (aerosol optical thickness values) an uncertainty of 2% is attached to the proposed method.* |
| | *Image quality / SNR is validated based on methods presented at the JACIE Workshop [RD.5]* |
| Reference | *See section 5.* |

For any assessment, the compliance between the validation results and data provider specification is shown in Table 2. Validation results demonstrates an overall agreement between satellite and reference measurements and agreement is in most cases within uncertainties claimed by the data provider.

All EDAP validation report are *in section 4.* Furthermore, the EDAP assessment have been performed independently from the satellite mission owner. As result, the EDAP grade if **Validation Results** is "*Good*".

**Table 2 -** EDAP Validation Assessment Results.

| EDAP Validation Assessment | Compliance (Y / N) |
|---|---|
| Product Documentation | Y |
| Product Format | Y |
| Image Quality / Visual Inspection | Y |
| Image Quality / Signal To Noise Ratio | Y |
| Image Quality / Modulation Transfer Function | Y |
| Geometric Quality / Absolute Geolocation | Y |
| Geometric Quality / Temporal Registration | Y |
| Geometric Quality / Interband Registration | Y |
| Geometric Quality / Stereoscopic Capability | *NA** |
| Radiometric Quality / Calibration | Y |

* As there is no input specification regarding stereoscopic capability (elevation accuracy), the compliance item has been set to Not Available (NA). In 4.7.6, the quality of the generated digital elevation model is discussed. EDAP assessment agree with accuracy results from scientific community (refer to [RD-24], [RD-26]), as discussed herein.

## 4. EDAP VALIDATION

### 4.1 Goals

Considering the innovative and often challenging technology associated with Very High Resolution (**VHR**) and High Resolution (**HR**) data, this Technical Note (**TN**) reports the results of the performed quality assessments with respect to the following validation aspects:

- Product Documentation
- Product Format Evaluation
- Image Quality
- Geometric Calibration Quality
- Radiometric Calibration quality.

### 4.2 Product Documentation Evaluation

The Planet products are in general extremely well detailed with the product User Guide document [RD-3] and Data Quality Report [RD-5].

### 4.3 Product Format Evaluation

The product evaluation is performed for any of the three product types listed below. The product format is detailed in [RD-3]. The EDAP team checks product format is in conformance with the format specification as defined by the data provider. Without going into details, we conclude that the product format is conformed.

Note that the accuracy assessments are performed by using Basic Scene Product (Level 1A) and Ortho Collect (Level 1C_C). The Ortho Scene Product is used to investigate issues found in the Ortho Collect Product.

**Basic Scene Product (Level 1A)**

The level 1A embeds the following images:

- Analytic - unorthorectified, radiometrically corrected, multispectral BGRN
- Analytic DN - unorthorectified, multispectral BGRN
- Panchromatic - unorthorectified, radiometrically corrected, panchromatic (PAN)
- Panchromatic DN - unorthorectified, panchromatic (PAN)
- L1A Panchromatic DN - unorthorectified, pre-super resolution, panchromatic (PAN)

The format of imagery files (including mask data) is GeoTIFF. The metadata format is JSON. There is also text file embedding Rational Polynomial Coefficients (RPC) information. Note that metadata information and even more is replicated into the Image GeoTIFF header (TIFFTAG_IMAGEDESCRIPTION).

**Ortho Scene Product (Level 1C)**

The level 1C embeds the following images:

- Visual - orthorectified, pansharpened, and colour-corrected (using a colour curve) 3-band RGB Imagery,
- Pansharpened Multispectral - orthorectified, pansharpened 4-band BGRN Imagery,
- Analytic - orthorectified, multispectral BGRN. Radiometric corrections applied to correct for any sensor artefacts and transformation to top-of-atmosphere radiance,
- Analytic DN - orthorectified, multispectral BGRN, uncalibrated digital number imagery product Radiometric corrections applied to correct for any sensor artefacts,

- Panchromatic - orthorectified, radiometrically correct, panchromatic (PAN),
- Panchromatic DN - orthorectified, panchromatic (PAN), uncalibrated digital number imagery product.

The format of imagery files (including mask data) is GeoTIFF. The metadata format is JSON. As for previous product type, metadata information and even more is replicated into the Image GeoTIFF header (TIFFTAG_IMAGEDESCRIPTION).

**Ortho Collect (Level 1C_C)**

The "Ortho Collect" images is defined as a composition of about 60 "Ortho scenes" products (20 per camera). There is no difference between Level 1C and Level 1C_C. The content is the same and previously defined above. The format of imagery files (including mask data) is GeoTIFF. The metadata format is JSON.

## 4.4 Image Quality: Visual Inspection

### 4.4.1 Activity Description Sheet

**Table 4-1: Activity description sheet for image quality visual inspection**

| Visual inspection |
| --- |
| *Inputs* |
| Set of Level 1C SKS data observed over La Crau (France) and PICS Libya 4 (Libya) (Regarding TDS List please refer to A.2) |
| *Description* |
| The visual inspection tasks includes assessment of the quick look images, assessment of the full resolution images and assessment of the mask.<br><br>In this context, the main tasks undertaken within this activity are:<br><br>• Check of the UDM<br>• Qualitative evaluation of Image interpretability |
| *Outputs* |
| Qualitative assessment of the image data information.<br>Image interpretability report<br>Assessment report on data mask |

### 4.4.2 Introduction

This visual inspection addresses three product components; the unusable data mask and image interpretability.

### 4.4.3 Unusable Data Mask

This section starts with a discussion on the consistency of the data mask accompanying image data.

For this purpose, any data mask images of the input test data set have been extracted from UDM / UDM2 files and analysed from visual and quantitative point of views. The UDM file provides information on areas of unusable data within an image (e.g. cloud and non-imaged areas). The content of the UDM image is explained in [RD-3]. The value of each pixel in the UDM is coded on 1 byte and is seen as a bit sequence, each bit set to 0 or 1 depending on the flagging rule. The UDM image pixel values are as follows:

- Bit 0: Identifies whether the area contains backfill in all bands,
- Bit 1: Identifies whether the area is cloud covered,
- Bit 2: Identifies whether the area contains missing (lost during downlink) or suspect (contains downlink errors) data in band 1,
- Bit 3: Identifies whether the area contains missing (lost during downlink) or suspect (contains downlink errors) data in band 2,
- Bit 4: Identifies whether the area contains missing (lost during downlink) or suspect (contains downlink errors) data in band 3,
- Bit 5: Identifies whether the area contains missing (lost during downlink) or suspect (contains downlink errors) data in band 4,

- Bit 6 is set to "0",
- Bit 7 is set to "0".

The UDM has been analysed and it has been observed that flags are not fully used, meaning that only bit related to cloud is set up. In addition, it has been noted that thin clouds are not detected.

## 4.4.4 Image Interpretability

For this assessment, points of interest (**POI**) are used to compare surface reflectance images (basic scene) and pansharpened images with reference high-resolution Pléiades (**PHR**) top of atmosphere images. This allows for the comparison of the detection of objects (delineation), the identification (interpretation) of objects, as well as the preservation of texture, to be performed. It is expected that the same level of details (i.e. the delineation and interpretation) of the same objects will be possible between SKS pansharpened and PHR imagery as they share the same 0.5 m pixel size.

The following products have been used for this assessment:

PHR Orthorectified (Multispectral)
PHR1B_201409251042136_FR1_PX_E005N43_0215_01048

(PHR data has been used, it is "true" 0.5 m multispectral data)

SKS Collect (Multispectral Analytic): 20210314_101355_ssc4_u0001

For this assessment, two sets of "full-resolution" quicklooks (i.e. no resampling or zoom applied) have been generated (one Blue, Green, Red colour composition and one Green, Red, NIR colour composition) and clipped around each POI (400 x 400 pixels).

All POIs are listed in the Table 4-2 below. Note for some POIs there is no data (smaller image) and POIs have not been extracted for all of the three images.

**Table 4-2: POI over the Salon scene**

| wkgt_geom (UTM 31) | Id | Description |
|---|---|---|
| Point (671090.3105554151115939 4830278.58671295549720526) | 1 | Modulation Transfer Function target |
| Point (671364.24309313111007214 4833044.0252351425588131) | 2 | Motor way / sharp transition (45° NE) |
| Point (668580.81736886233557016 4828965.45189037173986435) | 3 | Forest |
| Point (670056.62237295764498413 4828905.08180973120033741) | 4 | Roundabout / parking lot |
| Point (669985.90922565956134349 4832120.72269264236092567) | 5 | Elevated tree |
| Point (669956.03863696497865021 4832655.53592716064304113) | 6 | Motor way / roundabout |
| Point (670564.24590074480511248 4833363.40447467099875212) | 7 | The dam |
| Point (669836.88448120269458741 4832528.00618595350533724) | 8 | Big building (shadow) |

| wkgt_geom<br>(UTM 31) | Id | Description |
|---|---|---|
| Point (670518.95015854423400015<br>4829513.56928175128996372) | 9 | Landing track - 34 |
| Point (670249.72702971810940653<br>4831735.0312919020652771) | 10 | Floor Painting |
| Point (670900.38168655894696712<br>4829617.21182315889745951) | 11 | Crop fields / sparse |
| Point (671548.0352310094749555<br>4830292.1131860688328743) | 12 | Broadleaved woodland |
| Point (671099.93821095407474786<br>4828090.14610077627003193) | 13 | Crop fields |
| Point (671156.44116920174565166<br>4828825.77096180152148008) | 14 | Bridge and water |
| Point (671120.4438803291413933<br>4827691.31545618735253811) | 15 | Crop fields |
| Point (670328.31568091106601059<br>4831489.30539688002318144) | 16 | Building / EA 15 |
| Point (671516.86161747551523149<br>4833207.41657157335430384) | 17 | Greenhouse |
| Point (669996.87127304612658918<br>4829099.09009433817118406) | 18 | Parking lot |
| Point (670062.87681329366751015<br>4829781.35287734866142273) | 19 | Plane parking |
| Point (670860.46870227111503482<br>4831527.10888031311333179) | 20 | Plane hangar |
| Point (671802.47347140731289983<br>4832385.40385554917156696) | 21 | Small crop fields |
| Point (671246.59432400949299335<br>4832300.03732818737626076) | 22 | Urban city |

The results indicate the following:

1) The contrast of the multispectral bands at 0.5 m is degraded; blur is visible in the quicklooks and the original multispectral images which makes the identification of some objects at 1.0 m almost impossible (e.g. blurred car park shown in Figure 4-2, roof of buildings).
2) The pansharpening applied, in aim of restoring high frequency content (i.e. edges), performs well and data becomes more comparable with PHR data. However, it still remains difficult to identify / interpret objects in the SKS but not in the PHR imagery.
3) The pansharpening applied to SKS imagery is particularly useful for imagery of urban city landscapes (motorways, bridges, roundabouts, buildings, etc.) but as shown in the figures below, we cannot conclude that the 0.5 m SKS is equivalent to 0.5 m PHR in terms of image interpretability.

One drawback is that pansharpening does not preserve physical quantities. An additional drawback of pansharpening, which is well known in the user community and confirmed here, is the side effects of such processing, for example the low textured image regions are smoother compared to the original imagery, with the risk of skipping information (i.e. tree coverage, crop fields, and any other highly textured image information that can be assimilated to noise).
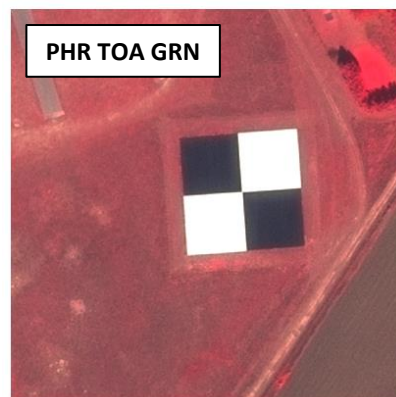
**Figure 4-1 POI 1, Green, Red, NIR Colour Composition.**

**SKS SR GRN**



**SKS PANSHARPENED GRN**



**PHR TOA GRN**

**Figure 4-2 - POI 19 (NIR, Red and Green colour composition).**

A POI image shows a comparisons between full resolution quicklook images; namely SKS pansharpened, SKS non-pansharpened, PHR non-pansharpened images.

A POI image displays quicklook images as follow;
- Top Left: RGB SKS pansharpened image,
- Top Right: RGB SKS non-pansharpened image,
- Bottom left: RGB PHR image.

The most relevant POI images have been selected and are shown here below, POI identifier as listed in Table 4-2, is also indicated. Note that the geographic extents of PHR and SKS
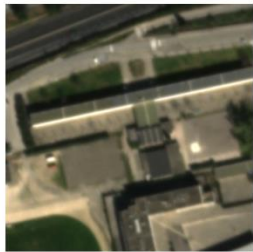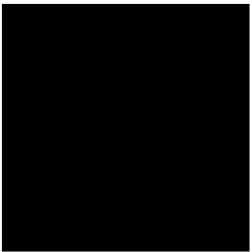
scenes are not totally similar. Also, for some POI, there is no corresponding image and the POI image.

| | |
|---|---|
| Top Left: | RGB SKS pansharpened image |
| Top Right: | RGB SKS non-pansharpened image |
| Bottom left: | RGB PHR image |
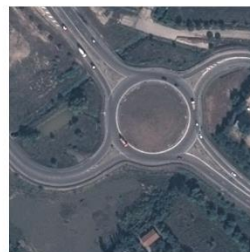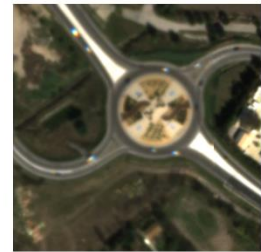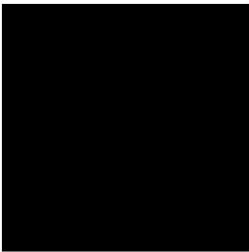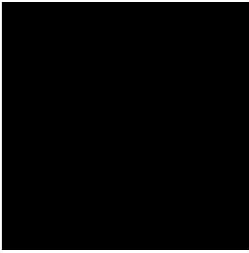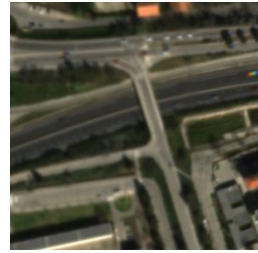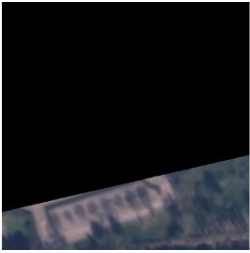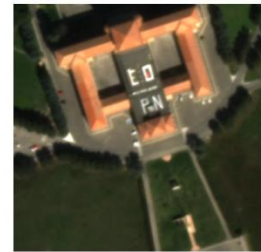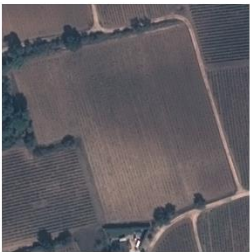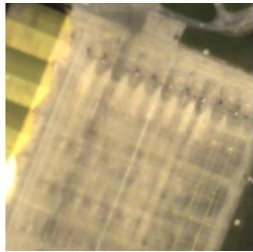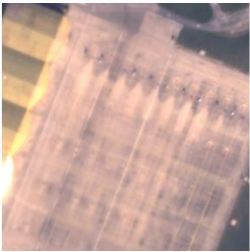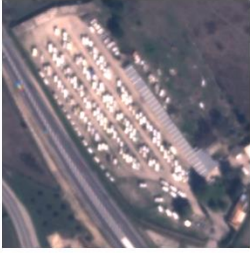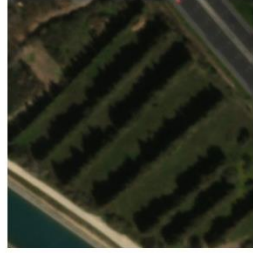
### 4.4.5  Conclusion

This preliminary assessment shows that image interpretability of the original and, more importantly, the pansharpened SKS imagery is slightly degraded (i.e. blurring and smoothing introduced) when compared to the PHR reference imagery.

## 4.5    Image Quality: Signal-to-Noise Ratio

This assessment proposes to validate the SKS SNR using data observed over the radiometrically bright target, PICS Libya 4.

### 4.5.1    Activity Description Sheet

| SNR Accuracy Validation |
|---|
| *Inputs* |
| Set of Level 1A SKS data (Basic scenes) observed over Libya 4 PICS site (set of products is listed in A.2) |
| *Description* |
| The SNR has been estimated for each spectral band. The data has been evaluated for a reference radiance corresponding to those of the Libya 4 desert site for the concerned spectral bands. |
| The Planet quality control team monitors SNR performance for all satellites and report results on a quarterly basis in [RD-5] by using statistics over differential SNR (gSNR) results. As defined in [RD-5], the gSNR formulation provides by Planet is not standard and a priori cannot be compared to EDAP results. |
| In [RD-7]; a mathematical relationship between gSNR and SNR is proposed. It is assumed herein, that this equation is applied for Planet, and it is point to be clarified with the data provider. |
| The gSNR results shared by Planet team for Q3 2020 are following ones: |
| • Blue: 34.398 <br> • Green: 42.703 <br> • Red: 45.399 <br> • NIR: 41.836 <br> • Pan: 173.605 |
| The gSNR minimal requirements for Blue / Green / Red is 30.0 and the gSNR requirements for Pan is 75.0 |
| Note that with the introduction of PBHDR imaging mode for all satellites, the planet quality team reports that the gSNR is improving. |
| There is no on board calibration device, more information on SNR assessment would be useful for cross-comparison purposes. |
| *Outputs* |
| The EDAP assessment provides SNR results for three satellites, considering several products (about 50). Results are consistent together and correct. Quantitative results are showing a slight degradation of SNR for 'SSC 1' which is confirmed by visual inspection. Very similar results are obtained for 'SSC 7' and 'SSC 10'. In addition, results are the same whatever the CCD number (1, 2, 3). |
| In addition, even if comparison between Planet and EDAP results are not straightforward, in both cases, the Red band SNR results are better than the Blue band ones. |

### 4.5.2  Introduction

The SNR is an important image quality indicator. Visual interpretation of image does not require high SNR data: even in presence of noise an operator is able to identify objects. However, multispectral image processing requires high SNR values in order to control as much as possible uncertainties in the measurement.

For each band, the SNR value and its corresponding average reference radiance $W.sr^{-1}m^{-2}$ are given. The proposed method herein has already been implemented in the context of other assessment. A description of method is given just here after.

### 4.5.3  Methods and Tools

The SNR is a measure of the mean signal to noise ratio. In the scientific community, there are two types of SNR typically measured; the temporal SNR and the spatial SNR. The basic formulation of the SNR is given by:

$$SNR = \frac{\mu}{\sigma}$$

Where:

o   $\mu$ is the mean signal,
o   $\sigma$ is the standard deviation of the signal.

The herein proposed method estimates the spatial SNR considering the statistical distribution over a set of "small windows" (9 pixels by 9 pixels), where by referring to the previous mathematical relationship:

• The "mean signal" is defined as the spatial average of a group of pixels in the "small window";
• Noise is typically defined as the standard deviation of a region of pixels in the "small window".

Each spectral band image (radiance measurement) is processed with the modified algorithm initially proposed in [RD-12]. The algorithm has been modified to allow the selection of small windows of uniform image intensity (condition 1), and the selection of small windows mostly located over regions with a flat terrain relief (condition 2).

For conducting this SNR assessment, a uniform / bright scene has been selected. The existing Libya-4 dataset, to be used for assessing absolute radiometric calibration accuracy later on, appears to be appropriate for this purpose. The site uniformity increases over small areas, and this is the reason for which small windows are selected. However, the spatial high frequency image content still exists, specifically at locations of sharp transitions (e.g. desert dune summit). To overcome this issue, a dedicated image processing is applied in order to detect high frequency content and filter small windows (image window processing with Sobel operator).

As a consequence, to fulfil both conditions, the proposed algorithm considers as input:

• Edge image, obtained with image processing (Sobel operator) to discard area with high frequency content
• DEM data

The different steps of this algorithm can be summarised as follows:

• Create SNR image, considering as input, image converted to radiance measurements, and iterating on "small windows" to compute SNR,

- Compute local statistics over 9 pixels x 9 pixels sliding window on the terrain relief data and the image edge response (Sobel Operator),
- Select the set of "small window" displaying uniform content and located in flat area
- Compute the statistical distribution (histogram) of "small windows" $\frac{\mu}{\sigma}$,
- Location of the peak in the histogram is a measure of the system SNR,
- Report the SNR value at the peak and the corresponding mean radiance value.
- Control SNR distribution with additional graphical representations.

The Figure 4-3 shows standard outputs used to control the proposed EDAP SNR method. This output includes following graphics:
- The top left graphic used to check that pixel selection is consistent; and one can expect a Gaussian distribution of values, stability of statistics against bin of radiance values,
- The bottom left graphic is used to appreciate how SNR is changing against bin of radiance values, one can expect very limited evolution within the considered radiance interval,
- The top right graphic is the histogram of selected pixel values,
- The bottom right graphic is the histogram of SNR (refer to step 4 in the previous description).

The top left graphic is based on the image of difference (DIFF) defined as the difference between input image and input image with uniform filtering applied. Also, the DIFF image exhibits high frequency content. When removing from DIFF image, signal due to edge, one can expect to get noise information.

The results shown in the bottom right and in the bottom left graphics, both are dealing with SNR. More confidence can be attributed to the bottom right one, because more measurements are taken into account (in the bottom left graphic, it is only per bin). As mentioned before, we expect, within radiance interval, very small changes affecting SNR curve (blue, bottom left graphic) and finally a mean value of the same order as the value deduced from 'snr cumul' (green, bottom right graphic), that is the location of the peak.
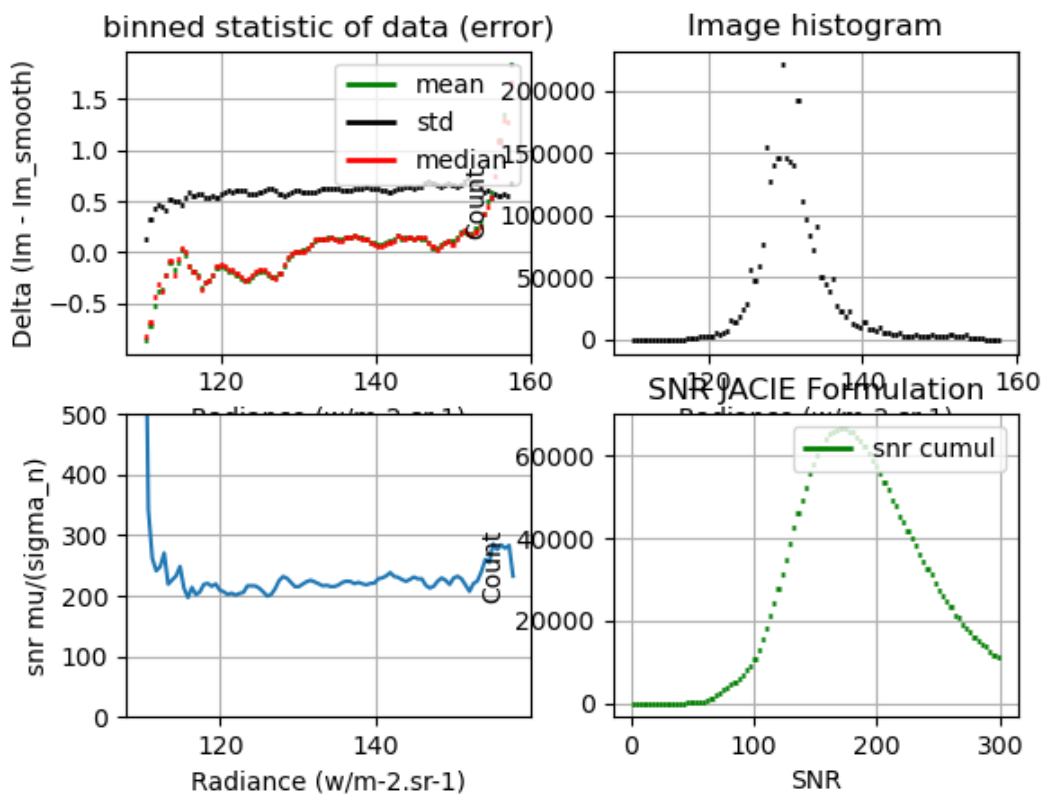


**Figure 4-3: Standard graphical outputs for SNR assessment.**

Input images are with a radiometric calibration applied, 16-bit DN pixel values correspond to radiance values which is particularly convenient for SNR computation. The TOA reflectance values are also computed.

The SNR is a function of the mean radiance of the landscape. The SNR is usually lower for low value of radiance (dark landscape) because the relative influence of the noise is larger. For large radiances, the SNR increases as the relative influence of the noise decreases.

We are working herein with a bright site, the SNR is expected to be high. As shown previously, the considered radiance intervals are quite small and does not allow to observe variations. Based on only one uniform test site, a noise model cannot be estimated.

The input product level is 1A, and EDAP did not apply additional geometric processing to express data within the instrument grid. As a result, column-wise noise and line-wise noise cannot be assessed separately.

The radiance measured and report in the SKS dataset is a top of atmosphere radiance. The SNR differs whether it is computed in radiances with or without atmospheric corrections. The scattering due to atmospheric constituent may have an impact on the SNR assessment. For the concerned scenes, the atmospheric parameters are listed in [A.4], the aerosol optical thickness varies within a range of 0.19 up to 0.28, which means an atmospheric transmittance between 82% and 75% according to [1]. In [RD-12], a rule for a rough estimation of the SNR uncertainty in case of radiances given without atmospheric corrections (Eq. 49), our case here.

With an SNR of about 180, a radiance due to scattering equal to 0.05 times ground radiances and atmospheric transmittance give above, a rough calculation indicates a level of uncertainty in the range of 11 up to 12. This level of uncertainty is confirmed with variability of SNR in the dataset: mean SNR is computed based on more than 50 images and standard deviation does not exceed 8 for all bands, as shown in Table 4-3.

As mentioned in the Activity Description Team, the Planet team provides SNR results expressed in term of differential SNR (gSNR). The gSNR is also called Signal Difference to Noise Ratio (SDNR) in the community. The formulation of gSNR shows in [RD-5] does not match with the standard definition given in [RD-7]. For this report, it is assumed that both formulations are equivalent and it should be confirmed by Planet team.

The $SDNR$ is computed as the ratio of the signal difference between two Lambertian surfaces and the noise. The two surfaces have reflectances $\rho = 0.15$ and $\rho = 0.07$. The noise is usually computed for the worst case, which is for the highest reflectance.

$$SDNR = \frac{S(\rho = 0.15) - S(\rho = 0.07)}{N(\rho = 0.15)}$$

Where:

- $S(\rho)$ is the signal for Lambert target with reflectance $\rho$
- $N(\rho)$ is the noise for Lambert target with reflectance $\rho$

The $SNR$ for a target with reflectance $\rho$ is defined as follow:

$$SNR = \frac{S(\rho)}{N(\rho)}$$

---

[1] *https://www.cnes-multimedia.fr/video/flash/edu/documents/calisphair/fiche%20mesure.pdf*

In [RD-7], a rough mathematical relationship between gSNR and SNR is proposed and this formulation is used to compute from the EDAP SNR results the gSNR results. This mathematical relationship is defined as follow:

$$SDNR \approx SNR(\rho) \cdot \frac{0.08}{\sqrt{0.15 \cdot \rho}} \qquad \text{(Eq. 1)}$$

### 4.5.4 Region of interest

The region of interest is within the Libya 4 site, and defined within the full image extent. The background values are discarded from the selection, and this region is common to both product observation data and the dimension is about 3000 pixels x 3000 pixels.

### 4.5.5 Data

The Input working data are described in Appendix, A.2. All data are observed over Libya 4 during September 2020 (four observation dates). Three satellites involved are, 'SSC 1', 'SSC 7' and 'SSC 10'.

### 4.5.6 Results

In Table 4-3, the $SNR$ results are given against a particular reference radiance and a particular reference reflectance (TOA). The **$SDNR$** results are computed based on .previously described equation (Eq.1). The SDNR is systematically above 57 for all bands and de facto above Planet validation results: products are confirmed with accuracy specification disclosed by the data provider.

The $SNR$ statistics are computed over a large dataset (more than 50 images). Results do not change depending on the CCD number. As mentioned above, results are within the uncertainty level specified just above.

**Table 4-3: SNR results**

| SKS Spectral Bands | Mean $SNR(\rho)$ | $SDNR$ | Std SNR | Reference RADIANCE | $\rho$ (TOA) | # Images |
|---|---|---|---|---|---|---|
| Blue | 134,04 | 57 | 7,78 | 118,33 | 0,23 | 52 |
| Green | 174,32 | 65 | 8,73 | 141,44 | 0,30 | 53 |
| Red | 203,98 | 68 | 7,84 | 158,35 | 0,38 | 53 |
| NIR | 190,55 | 58 | 7,40 | 134,48 | 0,46 | 53 |

We are interested in the SNR results depending on satellite. As shown in Figure 4-4, the SNR estimated with 'SSC 1' data is mainly below the SNR estimated with the 'SSC 7' / 'SSC 11'. Accounting for the model, the differences, for a given TOA reflectance, are not to be underestimated. It is particularly true for the Blue band and the Green band for which SNR difference exceed 30.
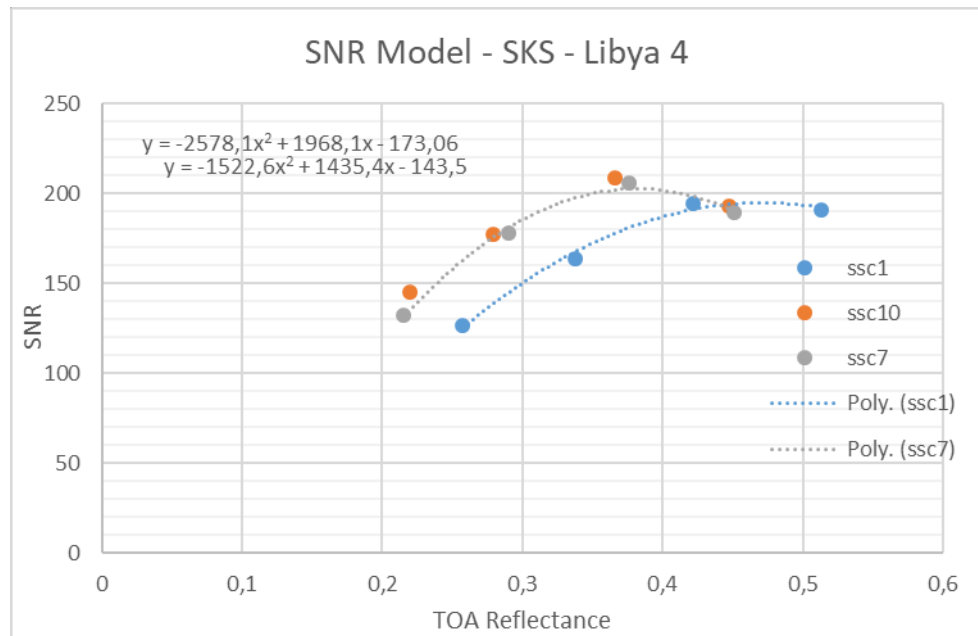
**Figure 4-4:** Mean SNR of each band for the three considered satellites.

A visual inspection confirms that for 'SSC-1' images magnitude of noise is greater than for 'SSC-7' / 'SSC-10' images. A reason of these discrepancies might be due to the atmosphere, however, as shown in [A.4], the atmospheric variables are stable with the concerned "SSC-1" observation period.

In the future, this EDAP method, proposed herein, should be played back with a larger dataset, including, in particular a diversity of landscape, it is a condition to better analyse noise structure.

### 4.5.7 Conclusions

This preliminary assessment shows that SNR results are mainly correct for all bands and whatever CCD. It demonstrates that radiometric equalisation between CCDs is correctly performed and for all configuration. However, there are also hypothesis according to which, accuracy is varying within the constellation, it is likely due to aging of the platform and so it is something to follow.

## 4.6    Image Quality: Modulation Transfer Function

This assessment proposes to estimate SKS image quality parameter; MTF, RER and FWHM. The method uses as input image of MTF artificial target located in Salon Airport (France).

### 4.6.1   Activity Description Sheet

| MTF Validation |
|---|
| *Inputs* |
| One level 1A SKS data (Basic scenes) observed over Salon Airport (MTF checkboard target) |
| *Description* |
| The EDAP MTF method is based on the slanted edge approach as described in [RD-14] (Telespazio method). The image quality parameter are estimated for each spectral band. <br><br> The Planet quality control team does not monitor MTF performance, rather the RER is monitored and results are report in on a quarterly basis in [RD-5]. The uncertainty results related to RER are: <br><br> • *Blue: 0.275* <br> • *Green: 0.301* <br> • *Red: 0.338* <br> • *NIR: 0.256* <br> • *Pan: 0.303* <br><br> Note that RER is *a good indicator of image sharpness.* |
| *Outputs* |
| The EDAP assessment provides image quality parameters for one product and the results indicates that the geometric resampling up to 0.5 m degrades image sharpness (confirming the results of the previous visual inspection assessment when dealing with non-pansharpened multispectral imagery). <br><br> The RER is quite stable across bands (0.07) and somehow degraded in the NIR band (0.05) |

### 4.6.2   Introduction

The spatial resolution of a sensor has traditionally been a difficult concept to define, but all would agree that it is inextricably linked to the GSD and Instantaneous Field of View (**IFOV**) of an imaging sensor system.

As a measure of the geospatial quality of imagery, the MTF of the system is often used along with the SNR. The MTF is often used as a measure of image sharpness. This important parameter for image quality has to be checked on each orbit in order to be sure that launch vibrations, transition from air to vacuum, or thermal state have not degraded the sharpness of the images [RD-14].

### 4.6.3  Methods and Tools

The slant-edge method presented herein has been developed and operated in the context of the ESA contribution to the ALOS PRISM calibration campaign [RD-15]. The different steps of the algorithm are depicted within Figure 4-5 below and discussed thereafter.
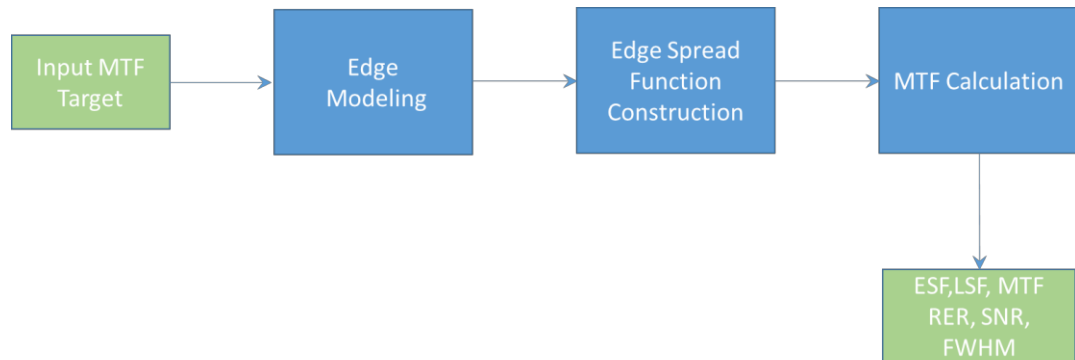


**Figure 4-5: Slant-edge method – algorithm steps.**

The input MTF target is a checkboard image observed in all spectral bands, an image of the target, observed with SKS is shown in Figure 4-6 (NIR spectral band, upper left image). The region of interest includes edge transitions, and nearly–vertical / nearly-horizontal edges are used to estimate MTF in the Along-track (**AL**) / Across-track (**AC**) direction or axis.

The method estimates for any spectral channels the MTF associated with the complete system response. The MTF is derived from computation of the ESF and Line Spread Function (**LSF**). These curves are accompanied with quality indicator metrics, such as RER, SNR and FWHM.

### 4.6.3.1  Edge Modelling

The true MTF is defined normal to the edge. If the edge is slanted, MTF is calculated from the average of many sampling phases.

The construction of the ESF is inspired from [RD-16] where sampling phases are collected for a given orientation of the target. The Edge modelling step is the estimation of the orientation of the target. As shown in Figure 4-6, for each image row included in the region depicted with rectangular form (Upper Left image), a parametric function is fitted in order to estimate the sub pixel location of the inflection point. Based on the set of inflection point sub pixel location found, a least square method is used to estimate an overall orientation angle (Upper right image): the rotation angle. The per-row interpolated edge functions (Lower Left image) are checked and discarded in case of noise.
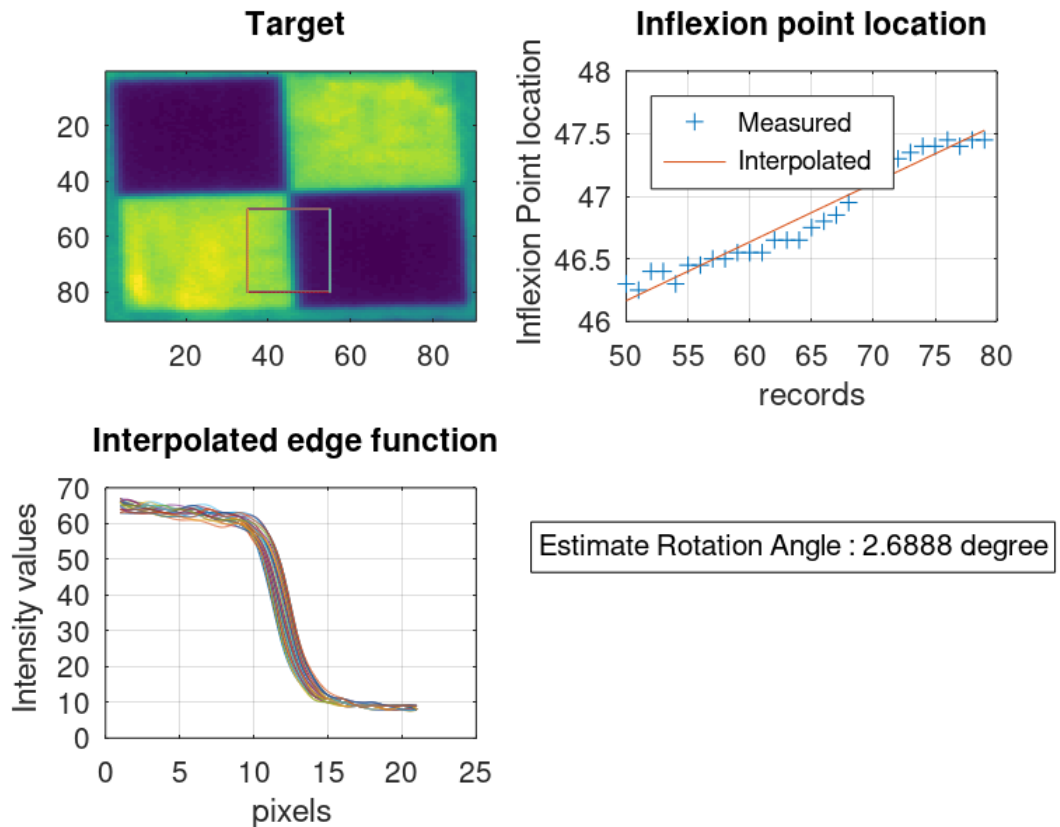
**Figure 4-6: Slant-edge method – edge modelling output (NIR band).**

### 4.6.3.2 Edge Spread Function Construction

The MTF method is very sensitive to noise and the orientation of edge should be accurately known. As mentioned before, a single image row is not sufficient to capture the various pixel phases accounting for aliasing and phase effects etc. The super resolved target image is built applying the same approach for each image row and following these stages;

- Projection of each image pixel onto a line perpendicular to edge applying rotation angle estimate in the previous step, the method proposed by Kohm [RD-16] is used;
- Resampling of the pixel position in the new projection system, within bin of ¼ pixel width.

Figure 4-7 shows the super resolved target image with edge transitions that are now perfectly aligned. Depending on the expected direction (Along / Across axis), it is possible to define for each bin, the intensity value (pixel phase) of the ESF. By nature, in the final ESF, some bins can be left empty or include very few measurements causing noise. For this reason, the orientation angle should be carefully selected.

Because some bins are definitely left empty, at this stage, the ESF data points are not uniformly distributed (not equally spaced). The LOESS curve fitting algorithm (locally weighted non-parametric regression fitting using a 2nd order polynomial) is used to resample the data to uniformly spaced sample points.

It is worth noting that the process does not fit a parametric model (sigmoid for instance) to the data points, the proposed approach herein is a non-parametric approach. More noise will be captured and results closer to the system behaviour.
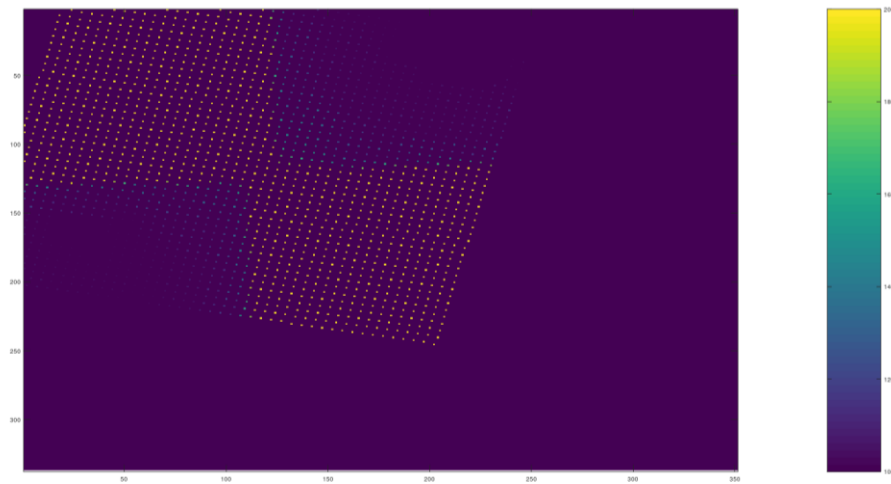
**Figure 4-7: Super Resolve Target (0.25 pixel bin).**

### 4.6.3.3    MTF Calculation

The final stage is to compute MTF by using a derivative method: computing the finite difference approximation of the uniformly spaced ESF to produce the LSF.

The LSF may contain high frequency noise, amplified by the derivative method. A local smoothing with fourth order Savitsky Golay filtering is applied (window size is 11 bins) to remove outliers. At the end, a Hann window is applied to the ESF (three-term weighted average smoothing technique) and a smooth LSF is obtained.

The main outputs of the method are shown in Figure 4-8 below and can be summarised as follow:

- The ESF – top left graphic,
- The LSF or ESF derivative – bottom left graphic,
- The MTF as LSF expressed in the Fourier domain – upper right graphic,
- The LSF together with LEOSS interpolated LSF, allowing to check intensity estimated for all empty bins – lower right graphic.

It is worth noting that in the ESF plot, variations located in the upper part of the curves are observed and these might be attributed to noise over uniform bright part of the checkboard. These variations are seen in the LSF plot, located in the right part outside the peak. The derivative filer is very sensitive to the noise, and therefore noise, impact strongly on the quality of measurement. These variations are seen in data from other HR EO missions and are mainly due to the quality of the checkboard target.
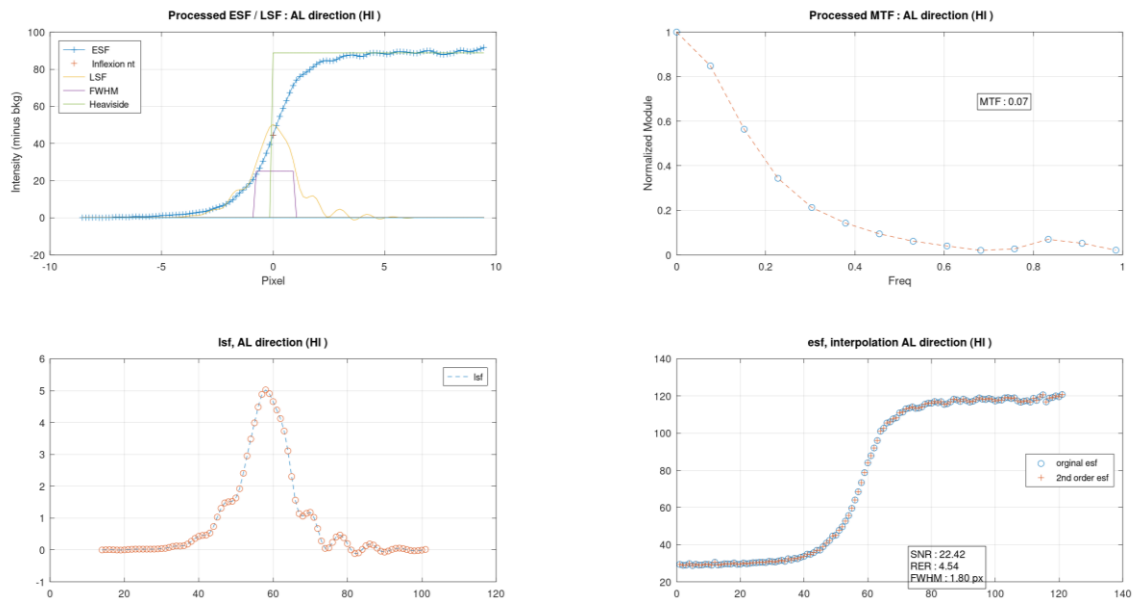
**Figure 4-8: Standard outputs of the MTF processing.**

### 4.6.4 Region of interest

The region of interest is Salon-de-Provence Airport, France. The MTF target seen by the SKS satellite is shown in Figure 4-9. When assessing MTF, it is done according to four directions. Also, the convention used to report MTF assessment is as follow:

- VL – Down **AL**ong track Edge, **V**ertical Edge from **L**ow to high luminance,
- VH – Up **AL**ong track Edge, **V**ertical Edge from **H**igh to low luminance,
- HL – Right **AC**ross track Edge, **H**orizontal Edge from **L**ow to high luminance,
- HH – Left **AC**ross track Edge, **H**orizontal Edge from **H**igh to low luminance.

### 4.6.5 Data

The Input working data are described in Appendix, A.2. The product used is 20201229_112916_ssc17d2_0018 with following properties:

- Level 1 Basic scene
- Optical System GSD 0.57 m
- Image pixel resolution 0.5 m
- Observed with SKS C17, launched in August 18, 2020 (Inclination: 53.0°)
- December day, haze (not mentioned in the metadata)

Images of the Salon MTF target are shown in figure just here below. It can be observed that uniform dark / bright image regions are not totally uniform, and so, it cannot be stated that target is a Lambertian surface. The quality of the artificial target is degraded, and artefacts seen are not due to SKS instrument. This issue makes our EDAP assessment less efficient (selection of suitable regions more difficult) and reliable (additional noise introduced in the computation).
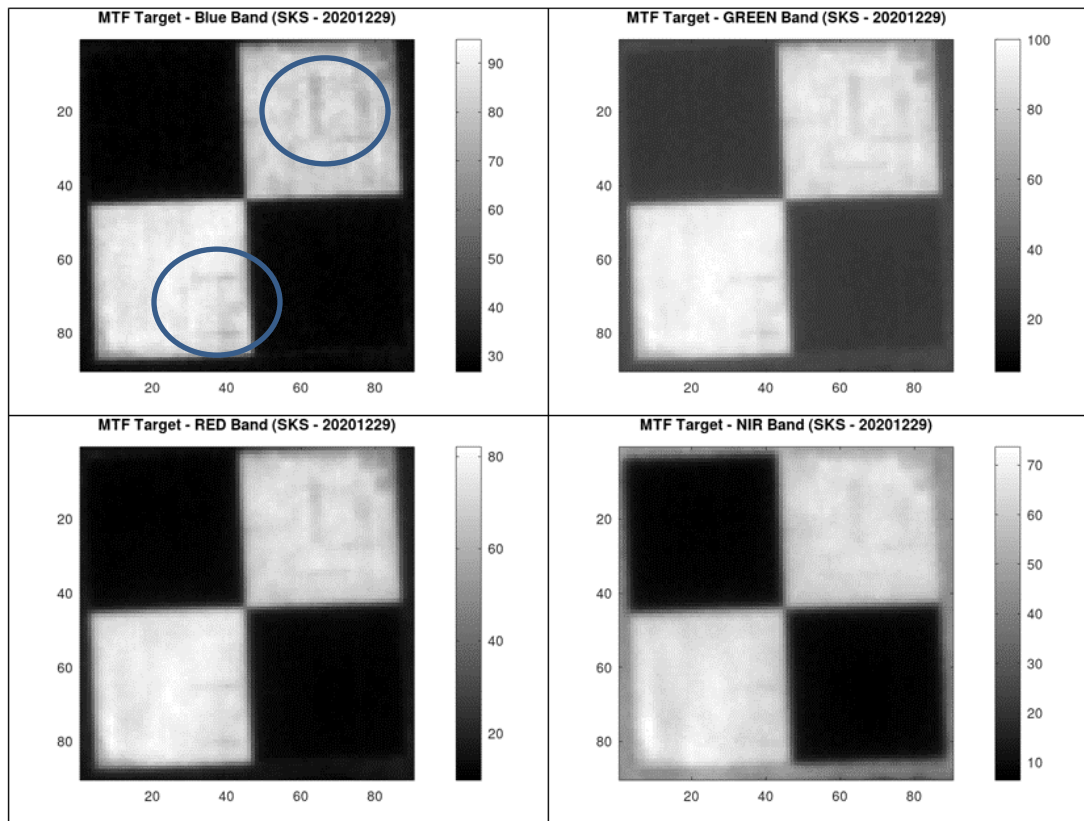
Figure 4-9: **SKS Images (December 29 2021) of the MTF target at Salon Airport and some visible degradations (blue circles)**

### 4.6.6 Results

As mentioned before, the quality of the target does not allow to reach a good estimate of quality parameters. Results remains interesting to be inter compared among bands and with regards to processing options. One can note that:

- Results are stable whatever the MTF direction
- FWHM is always above 2 pixels which might indicate blurring in case of perfect artificial target.
- RER is always below 1 and a bit below for the NIR bands
- MTF is always below 0.07
- The image quality is better for the Blue band and degraded progressively in the Green, Red and NIR bands.

The RER is a good indicator of image sharpness and remains very stable whatever the spectral band. It means that the method is consistent.

There is no agreement between the EDAP RER results and the Planet team ones. Results show that sharpness is degraded with the 0.5 m resampling.

The detailed results are listed in table below, the convention regarding edge profile direction (HH, LL, VH, VL) is specified just here before in 4.6.4.

**Table 4-4: MTF Results**

| Spectral Bands | Direction | MTF Along Track | | MTF Across Track | |
|---|---|---|---|---|---|
| | | HH | HL | VH | VL |
| Blue | SNR | 21 | 15 | 10 | 12 |
| | FWHM | 2,5 | 2,25 | 2 | 2,5 |
| | RER | 0,074 | 0,078 | 0,071 | 0,067 |
| | MTF@Nyquist | 0,05 | 0,04 | 0,06 | 0,05 |
| Green | SNR | 25 | 15 | 11 | 12 |
| | FWHM | 2,5 | 2,5 | 2,25 | 2,5 |
| | RER | 0,071 | 0,071 | 0,067 | 0,064 |
| | MTF@Nyquist | 0,035 | 0,034 | 0,045 | 0,035 |
| Red | SNR | 21 | 13 | 12 | 10 |
| | FWHM | 2,5 | 2,5 | 2 | 2,25 |
| | RER | 0,065 | 0,650 | 0,650 | 0,061 |
| | MTF@Nyquist | 0,04 | 0,025 | 0,035 | 0,031 |
| NIR | SNR | 17 | 12 | 12 | 10 |
| | FWHM | 2,5 | 2,75 | 2,5 | 2,25 |
| | RER | 0,059 | 0,057 | 0,058 | 0,058 |
| | MTF@Nyquist | 0,03 | 0,03 | 0,02 | 0,04 |

### 4.6.7 Conclusions

The MTF assessment confirms feedbacks of visual inspection assessment when dealing with multi spectral image with no sharpening applied. The Planet quality team results are more likely related to pansharpened products. It should be clarified in the future and procedure played back with more dataset.

The current EDAP MTF results indicates that the radiometric resampling up to 0.5 m degrades image sharpness.

## 4.7 Geometric Calibration Validation

This assessment proposes to validate geometric specification of the SKS family for the three different product types, mentioned above. Since Ortho Scene and Ortho Collect products are geometrically identical, only the latter one was assessed here. For this purpose, distinct methodologies have been set up and following geometric data quality aspects addressed:

- Absolute (planimetric) georeferencing accuracy obtained from the panchromatic imagery (panchromatic and pansharpened) as is (no improvements with sensor models and GCPs were applied).
- Temporal accuracy (between two acquisitions at Ortho Collect product level)
- Multispectral Interband registration (between the multispectral bands of Basic Scene Product)
- Stereoscopic (DSM generation) capability

### 4.7.1 Activity Description Sheet

## Geometric Accuracy Validation: Absolute / Temporal / Inter-band registration

### Inputs

Set of Level 1A & Level 1C_C SKS data observed over Ankara site acquired at three different dates (set of products is listed in A.2)

GCP Reference Vector layer ("Ankara") with 44 ground control points

UAV datasets taken over three test sites (each 1 km x 1 km) with RGB camera images (3 cm GSD) and MS camera images (11 cm GSD). Very dense Digital Surface Models and very high resolution orthophotos were produced for the three sites.

### Description

Estimation of the geometric accuracy of SKS products including absolute accuracy, multi temporal accuracy and inter-band registration accuracy.

Verification that measured geometric accuracy is within the product specification accuracy, as stated in the product specification document [RD-3] and regularly monitored by Planet in the quarterly report [RD-5].

The input product specifications (Level 1A, Level 1C, Level 1C_C) related to geometry is given in [RD-3] and is focused on the positional accuracy. The geometry differs depending on the processing level. *"The positional accuracy is better than 10.0 m RMSE"* for the Level 1C and 1C_C products. For the Scene (Level 1A) product, the accuracy specification is given as < 50 m.

The product accuracy results (Level 1C), report by the Planet quality control team, and considered as EDAP input specifications are given in [RD-5] and can be summarised as follows:

- *The absolute geolocation accuracy is 3.4 m / 2.6 m  (Mean / STD RMSE accuracy), this average accuracy is computed based on 50139 products,*

- *The temporal geolocation accuracy is 3.1 m / 5.7 m (Mean / STD RMSE accuracy), this average accuracy is computed based on 55496 products,*

- *The Inter-band registration accuracy (Mean / STD RMSE Accuracy) is summarised as follow:*

  *Blue - Green : 0.11 m / 0.06 m*

  *Blue - Red    : 0.13 m / 0.08 m*

  *Blue - NIR    : 0.22 m / 0.14 m*

  *Green - Red  : 0.09 m / 0.05 m*

  *Green - NIR   : 0.20 m / 0.12 m*

  *Red -/ NIR    : 0.18 m / 0.12 m*

  *This average accuracy is computed based on about 63900 products.*

The DEM generation accuracy (Z-accuracy) obtained from SKS triplets was about 4 m reflected by the standard deviation value and 5.3 m normalised median absolute deviation value after a comparison with LiDAR data in [RD-24]. [RD-26] reported 1 to 2 m relative and 2 to 3 m absolute vertical accuracy of SKS triplet DEMs compared to reference airborne LiDAR and WorldView stereo DEMs.

### Outputs / Summary Results

| Geometric Accuracy Validation: Absolute / Temporal / Inter-band registration |
| --- |

*The geometric accuracy results over Ankara test site can be summarised as follows:*

- *The absolute geolocation accuracy of basic scene products in planimetry is 1.7 m / 1.3 m / 1.7 m (Mean / STD / RMSE accuracy). This accuracy is computed based on two basic scene products. The values are better than the specifications given above.*

- *The absolute geolocation accuracy of ortho collect products in planimetry is 1.4 m / 1.1 m / 1.2 m (Mean / STD / RMSE accuracy). This accuracy is computed based on two ortho collect products. The values are better than the specifications given above.*

- *The multi temporal geolocation accuracy is 1.8 m / 1.4 m / 1.5 m (Mean / STD / RMSE accuracy). This accuracy is computed based on 2 ortho collect products. The values are better than the specifications given above.*

- *The Inter-band registration accuracy (Mean / STD RMSE Accuracy) is summarised as follow:*

    *Blue - Green : 0.03 m / 0.02 m*

    *Blue - Red     : 0.07 m / 0.05 m*

    *Blue - NIR     : 0.12 m / 0.05 m*

    *This accuracy is computed based on six basic scene products. The values are better than the specifications given above.*


*The DEM generation accuracy (Z-accuracy) obtained from SKS triplets was 0.55 mean shift in height with 2.2 m STD as compared with the UAV DSM. The values obtained here are better than [RD-24], and in line with [RD-26]. The [RD-24] has a large temporal difference between the SKS and the reference DEM, which explains the larger deviation.*

### 4.7.2 Introduction

In this section dedicated to the assessment of geometry, there are four assessments performed: absolute accuracy, temporal accuracy, inter-band accuracy and stereoscopic capability. Results from additional qualitative checks are given in the last part.

### 4.7.3 Absolute Geolocation Accuracy

#### 4.7.3.1 Methods

The methodology for the absolute geolocation accuracy assessment is based on external reference, i.e. GCPs surveyed by using Global Navigation Satellite System (**GNSS**) instruments, over Ankara (Turkey) test site. A total of 44 GCPs were selected on the SKS Collect (ortho level) multispectral data and measured on the ground. The evaluations were carried out by using the following methods:

- Basic Scene products (2D assessment): backprojection of GCP ground coordinates to the panchromatic image coordinates using RPC files provided by the vendor; and comparative evaluation of the backprojected coordinates with the measured image coordinate values in x (row) and y (column) directions by using statistical metrics (i.e. mean, absolute mean, median, standard deviation and RMSE). See Figure 4-10 for the basic depiction of the RPC backprojection method. The input of the coordinate transformation function for every point is Latitude, Longitude and Height values and the given RPCs are used in the rational polynomial functions with the inputs. The output of the backprojection function is line and sample (or row and column) coordinates in image space.

- Ortho Collect products (2D assessment): Measurement of GCP coordinates from the orthorectified images and comparison with the ground coordinates in X and Y directions by using statistical metrics (i.e. mean, absolute mean, median, standard deviation and RMSE).
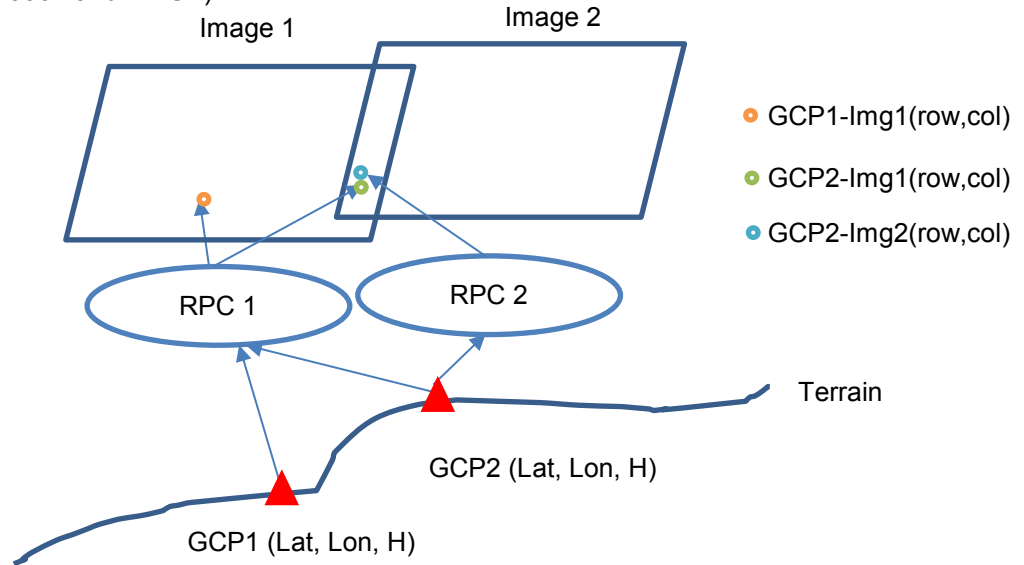


**Figure 4-10: RPC backprojection method.**

### 4.7.3.2 Data

The data used for the geolocation assessment involve SKS Scene and Collect products (Table 4-5) and a total of 44 GCPs surveyed with GNSS instruments. Although 6 other GCPs exist in the area, they do not fall into the footprint of the SKS products. All GCP locations are shown on the SKS Collect product from 18 July 2021 in Figure 4-11.

**Table 4-5: SKS data used for the absolute geolocation assessment**

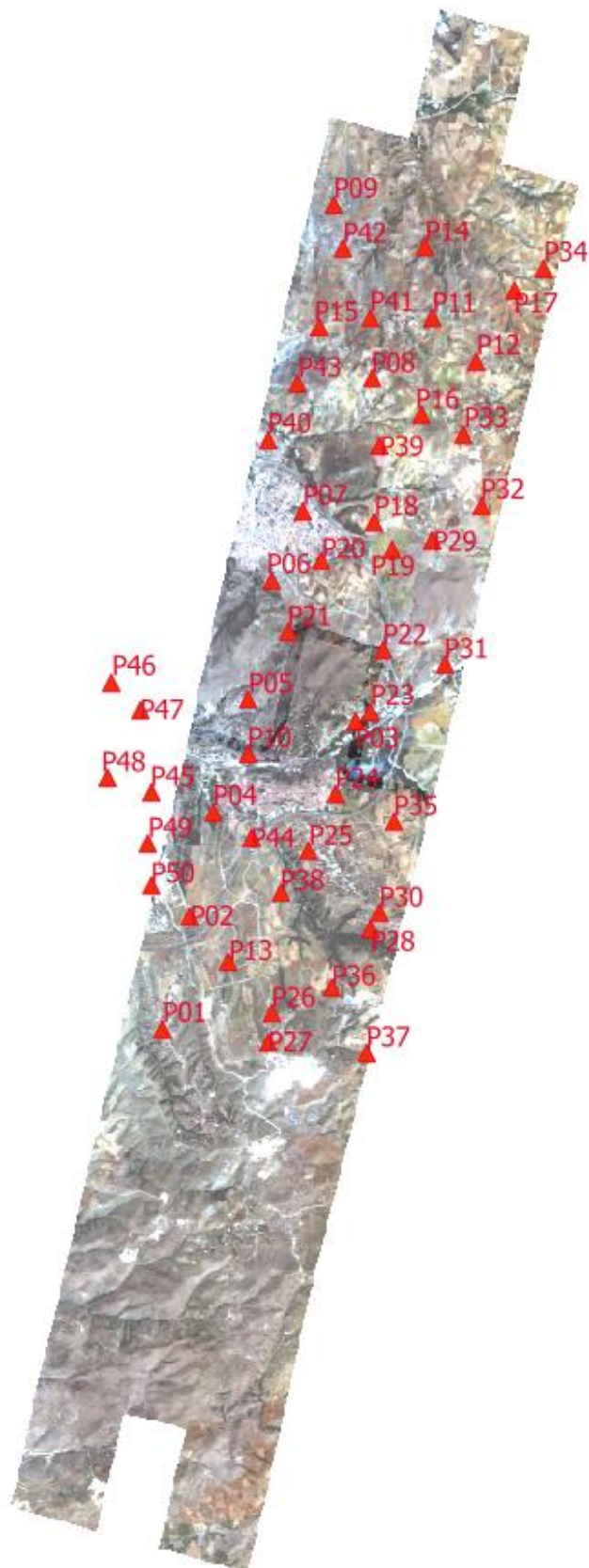| Product Level | Bands & GSD | Acquisition Date and Satellite |
|---|---|---|
| Basic Scene products with RPCs | Panchromatic band with 73 cm GSD | 18 July 2020 (SKS4) |
| Ortho collect products | 4 MS bands with 50 cm GSD | 18 July 2020 (SKS4) |
| Basic Scene products with RPCs | Panchromatic band with 66 cm GSD | 23 Sep 2020 (SKS7) |
| Ortho collect products | 4 MS bands with 50 cm GSD | 23 Sep 2020 (SKS7) |

**Figure 4-11: The distribution of GCPs over Ankara, test site and the SKS Collect data (image transparency is used for visualization purposes) from 18 July 2020.**

### 4.7.3.3    Results

**Table 4-6: Planimetric Accuracy Results of SKS Collect RGB image from18 July 2020 (Absolute, in meter unit).**

| Reference | GCP Set |
|---|---|
| Working  Image (SKS Collect RGB 50 cm) | Image mosaic of 18 July 2020 |
| Sample (#GCP) | 44 |
| Easting Error Mean (m) | -0.65 |
| Northing Error Mean (m) | -0.16 |
| Easting Error STD (m) | 1.38 |
| Northing Error STD (m) | 1.21 |
| **Easting Root Mean Square Error (m)** | **1.52** |
| **Northing Root Mean Square Error (m)** | **1.22** |
| **Root Mean Square Error (m)** | **1.38** |
| **Circular Error @ 90 Percentile (m)** | **2.89** |

**Table 4-7: Planimetric Accuracy Results of SKS Collect RGB image from 23 Sep 2020 (Absolute, in meter unit).**

| Reference | GCP Set |
|---|---|
| Working  Image (SKS Collect RGB 50 cm) | Image mosaic of 23 Sep 2020 |
| Sample (#GCP) | 43 |
| Easting Error Mean (m) | 0.08 |
| Northing Error Mean (m) | -0.39 |
| Easting Error STD (m) | 0.74 |
| Northing Error STD (m) | 0.95 |
| **Easting Root Mean Square Error (m)** | **0.74** |
| **Northing Root Mean Square Error (m)** | **1.03** |
| **Root Mean Square Error (m)** | **0.90** |
| **Circular Error @ 90 Percentile (m)** | **1.23** |

**Table 4-8: Planimetric Accuracy Results of SKS Scene Pan image from 18 July 2020 (Absolute, in meter unit).**

| Reference | GCP Set |
|---|---|
| Working Image (SKS Scene Pan + **RPC**) | Pan image of 18 July 2020 |
| Sample (#GCP) | 43 |
| Easting Error Mean (m) | -0.64 |
| Northing Error Mean (m) | 1.06 |
| Easting Error STD (m) | 1.23 |
| Northing Error STD (m) | 1.50 |
| **Easting Root Mean Square Error (m)** | **1.39** |
| **Northing Root Mean Square Error (m)** | **1.84** |
| **Root Mean Square Error (m)** | **1.63** |
| **Circular Error @ 90 Percentile (m)** | **4.03** |

**Table 4-9: Planimetric Accuracy Results of SKS Scene Pan image from 23 Sep 2020 (Absolute, in meter unit).**

| Reference | GCP Set |
|---|---|
| Working Image (SKS Scene Pan + **RPC**) | Pan image of 23 Sep 2020 |
| Sample (#GCP) | 39 |
| Easting Error Mean (m) | 0.21 |
| Northing Error Mean (m) | 0.42 |
| Easting Error STD (m) | 1.32 |
| Northing Error STD (m) | 1.13 |
| **Easting Root Mean Square Error (m)** | **1.33** |
| **Northing Root Mean Square Error (m)** | **1.21** |
| **Root Mean Square Error (m)** | **1.27** |
| **Circular Error @ 90 Percentile (m)** | **2.45** |

### 4.7.4  Temporal Geolocation Accuracy

#### 4.7.4.1    Methods

As a preliminary assessment, the multi-temporal accuracy was evaluated by comparing the coordinate differences obtained from the manually measured GCP coordinates on two Collect Ortho products.

In addition, for the temporal assessment, the geometric grids of two images acquired at a different time and with two different SKS satellites are compared. The products involved in this assessment are listed in table just here after. The view angles of 18 July 2020 Ortho Collect Products are 20.2° and 16.6° degrees. The view angles of 23 September 2020 products are 1.8° and 3.8° degrees.

The grid comparison is performed by using a classic image matching approach relying on an intensity-based method. The method performs statistical analysis of the image matching outputs: the geometric displacements between the two image grids computed for each pixel are analysed. The accuracy of the method is within 0.1 pixel.

A drawback of this method is the selection of the most confident measurements involved in the accuracy assessment, discarding in particular noisy results, and cloudy pixels.

The assessment is performed on the Red band images and results report accordingly. The Red band image offers a better contrast and a higher SNR. Also information to be matched is increased.

It is worth noting that regarding the other Blue, Green, Red, NIR images, the results on inter-band registration given later in the document can then be used to derive the temporal accuracy for the other spectral bands.

#### 4.7.4.2    Data

**Table 4-10: SKS data used for the temporal geolocation assessment**

| Product Level | Bands & GSD | View angles | Acquisition Date and Satellite |
|---|---|---|---|
|  |  |  |  |

| Ortho collect products | 4 MS bands with 50 cm GSD | 20200718_082806_ssc4_u0001: 20.2° 20200718_082806_ssc4_u0002: 16.6° | 18 July 2020 (SKS4) |
|---|---|---|---|
| Ortho collect products | 4 MS bands with 50 cm GSD | 20200923_112354_ssc7_u0002: 1.8° 20200923_112354_ssc7_u0001: 3.8° | 23 Sep 2020 (SKS7) |

In addition, a total of 43 GCPs surveyed with GNSS instruments as explained in the previous section was used for GCP-based comparison.

### 4.7.4.3    Results

The results obtained from the image matching of 1193 points and manual measurements of 43 GCPs show that the results are compatible. The manual measurements have lower precision in comparison to the image matching method used here. The differences between the two results are within the noise level of the manual measurements. The matching method used here is reliable to assess the multi-temporal accuracy.

**Table 4-11: Temporal Geolocation Accuracy Results (in meter unit).**

| | |
|---|---|
| Reference Image (Red) | 18 July 2020 |
| Working Image (Red) | 23 Sep 2020 |
| Sample (#Pixel) | 1193 |
| Correlation Confidence | 0.90 |
| Easting Error Mean (m) | -0.36 |
| Northing Error Mean (m) | 0.48 |
| Easting Error STD (m) | 1.10 |
| Northing Error STD (m) | 1.05 |
| **Easting Root Mean Square Error  (m)** | 1.15 |
| **Northing Root Mean Square Error  (m)** | 1.15 |
| **Root Mean Square Error (m)** | 1.15 |
| Circular Error @ 90 Percentile (m) | 2.00 |
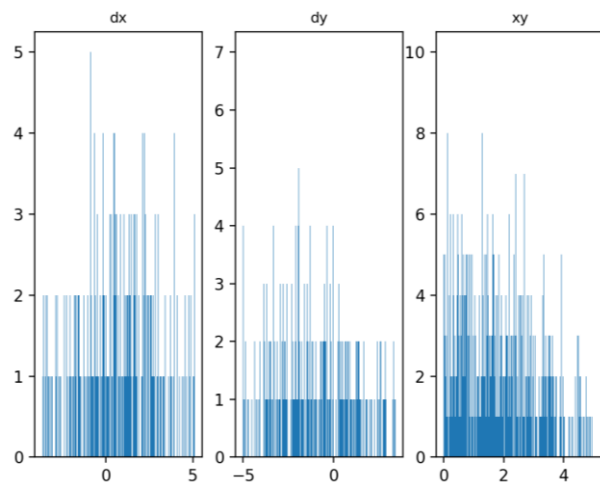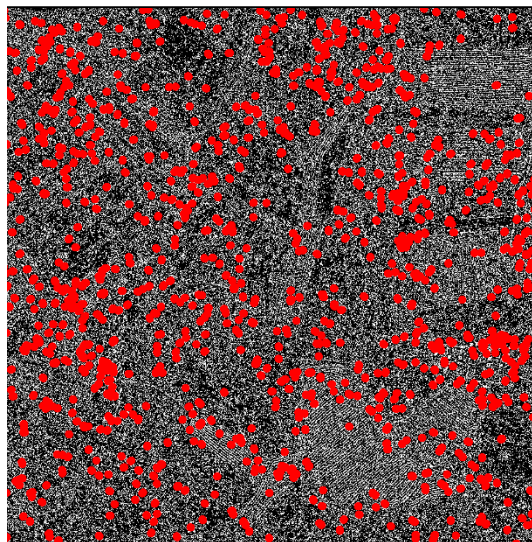
**Figure 4-12: Temporal Geolocation Accuracy – spatial distribution of automatically matched points (left) and the histograms of displacement errors; in line direction (X) / in pixel direction (Y) / in planimetry (XY) (right).**

**Table 4-12: Temporal Geolocation Accuracy Results obtained from GCPs.**

| | |
|---|---|
| Reference Image (SKS Collect RGB 50 cm) | 18 July 2020 |
| Working Image (SKS Collect RGB 50 cm) | 23 Sep 2021 |
| Sample (#GCP) | 43 |
| Easting Error Mean (m) | -0.72 |
| Northing Error Mean (m) | 0.27 |
| Easting Error STD (m) | 1.62 |
| Northing Error STD (m) | 1.16 |
| **Easting Root Mean Square Error  (m)** | **1.77** |
| **Northing Root Mean Square Error  (m)** | **1.19** |
| **Root Mean Square Error (m)** | **1.51** |
| Circular Error @ 90 Percentile (m) | 3.46 |

## 4.7.5  Inter-band Geolocation Accuracy

### 4.7.5.1    Methods

The objective is to assess the coregistration between bands. For a given product, several band twins are considered, namely (Blue, Green), (Blue, Red), (Blue, NIR), and geometry of the two image grids in the twin are compared. The grids are compared by using dense image matching technic: for any pixel location in the image space, a displacement, $D$, in both line (y) / pixel (x) direction is computed.

The post processing of image matching result is an essential stage before producing accuracy statistics and the related error budget.

Note that, the pan band was not used for the interband assessments of Basic Scene products due to the sensor design differences between the pan and the MS. The pan is a frame sensor with a different perspective effect than the MS bands, which are linear array sensors.

### 4.7.5.2    Data

**Table 4-13: SKS data used for the interband geolocation assessment**

| Product Level | Bands & GSD | Acquisition Date and Satellite |
|---|---|---|
| Basic Scene products with RPCs | MS bands with 73 cm GSD | 18 July 2020 (SKS4) |
| Basic Scene products with RPCs | MS bands with 66 cm GSD | 23 Sep 2020 (SKS7) |

An overview of the three MS bands is from 18 July 2020 dataset is shown in Figure 4-13.

**Figure 4-13: Basic scene products used for the interband evaluations from 18 July 2020.**

### 4.7.5.3 Results

As given in the activity description sheet, the inter-band registration accuracy, claimed by the data provider, depends on the band twin. We do not assess accuracy of all band twins. It is expected that the accuracy results found is below Mean RMSE + STD RMSE. This information is added in Table 4-14 and comes in the table row with text written bold type.

Table 4-14 and Table 4.14 below provides inter-band accuracy results of one Basic Scene results from the two acquisitions. For each band twins (Reference Band/ Working Band) the geometric uncertainties derived from statistical processing is provided. The results of four other processed scenes were similar and thus the detailed results are not included here. A summary of all interband results are given in Section 4.7.7.

Table 4-14 below provides inter-band accuracy results. For each band twins (Reference Band/ Working Band) the geometric uncertainties derived from statistical processing is provided.

From statistics point of view, the centring accuracy is correct. The STD is always within 2.0 m in both Easting and Northing directions. All RMSE values are below the proposed specification.

**Table 4-14: Inter-band registration results from 18 July 2020 dataset (20200718_082806_ssc4d1_0009_basic_analytic.tif).**

| Reference Band | Blue | Blue | Blue |
|---|---|---|---|
| Working Band | Green | Red | NIR |
| Sample (#Pixel) | 17508 | 15170 | 10287 |
| Easting Error Mean (m) | 0.73 | 0.73 | 0.73 |
| Northing Error Mean (m) | -0.01 | -0.01 | -0.06 |
| Easting Error Std  (m) | 0.00 | -0.07 | -0.01 |
| Northing Error Std (m) | 0.04 | 0.04 | 0.07 |
| Easting Error RMS  (m) | 0.04 | 0.05 | 0.07 |
| Northing Error RMS (m) | 0.04 | 0.04 | 0.09 |
| Root Mean Square Error (m) | 0.04 | 0.08 | 0.07 |

**Table 4-15: Inter-band registration results from 23 Sep 2020 dataset (20200923_112354_ssc7d1_0012_basic_analytic.tif).**

| Reference Band | Blue | Blue | Blue |
|---|---|---|---|
| Working Band | Green | Red | NIR |
| Sample (#Pixel) | 19093 | 15925 | 16440 |

| | | | |
|---|---|---|---|
| Easting Error Mean (m) | 0.02 | 0.02 | 0.01 |
| Northing Error Mean (m) | -0.02 | -0.03 | 0.09 |
| Easting Error Std  (m) | 0.03 | 0.03 | 0.05 |
| Northing Error Std (m) | 0.03 | 0.03 | 0.06 |
| Easting Error RMS  (m) | 0.03 | 0.03 | 0.05 |
| Northing Error RMS (m) | 0.03 | 0.05 | 0.11 |
| Root Mean Square Error (m) | 0.05 | 0.06 | 0.11 |

### 4.7.6  Stereoscopic Capability

#### 4.7.6.1    Methods

The stereoscopic capability was evaluated by producing DSM from three datasets. The PCI Geomatics software, Ontario, Canada, was used for the RPC improvement with 6 GCPs and DSM generation with semi-global matching (SGM) method. The comparison of the DSMs was carried out using the LS3D software from 4Dixplorer AG, Switzerland. The results were assessed in terms the elevation displacement obtained after the least squares surface matching and the sigma naught quantitatively. Visual assessments on the results were also carried out via color-coded residual map in 3D.

#### 4.7.6.2    Data

| Sensor | Product Level | Bands & GSD | Acquisition Date |
|---|---|---|---|
| SKS | Scene (individual frames with RPCs) | 4 MS bands -1 m<br><br>1 m<br><br>60 cm | 23 Sep 2020 (SKS7)<br><br>18 July 2020 (SKS4)<br><br>27 Sep 2020 (SKS12, only a small part) |

#### 4.7.6.3    Results

The DEM generation and comparison results within EDAP show that the accuracy is related to the temporal differences between the images, image off-nadir configuration, and the improvement of the RPCs using GCPs. Most state-of-the-art software use semi-global matching approach for DEM generation. The method relies on epipolar images, which can be produced by using precise RPCs.

A total of 6 GCPs were used for the RPC correction of 8 Basic Scene images acquired on three different dates. The DEM was produced by using these three acquisitions of the same area and the compared with the UAV DEM. The global shift between the SKS DEM and UAV DEM was 0.6 m in height, and the standard deviation of the residuals was 2.4 m. These results are in line with the literature [RD-24], [RD-26]. The residual map obtained from the comparison of UAV DSM (Figure 4-14) and the SKS DSM (Figure 4-15) are presented in Figure 4-16.
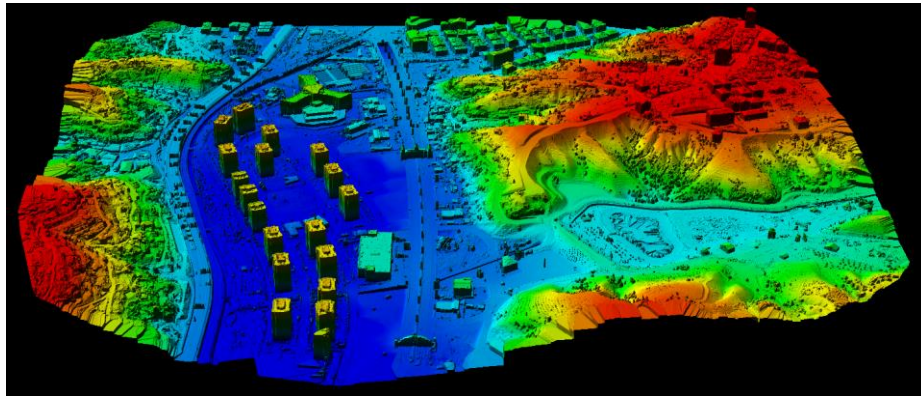
**Figure 4-14: UAV DSM over Ankara Test Site.**
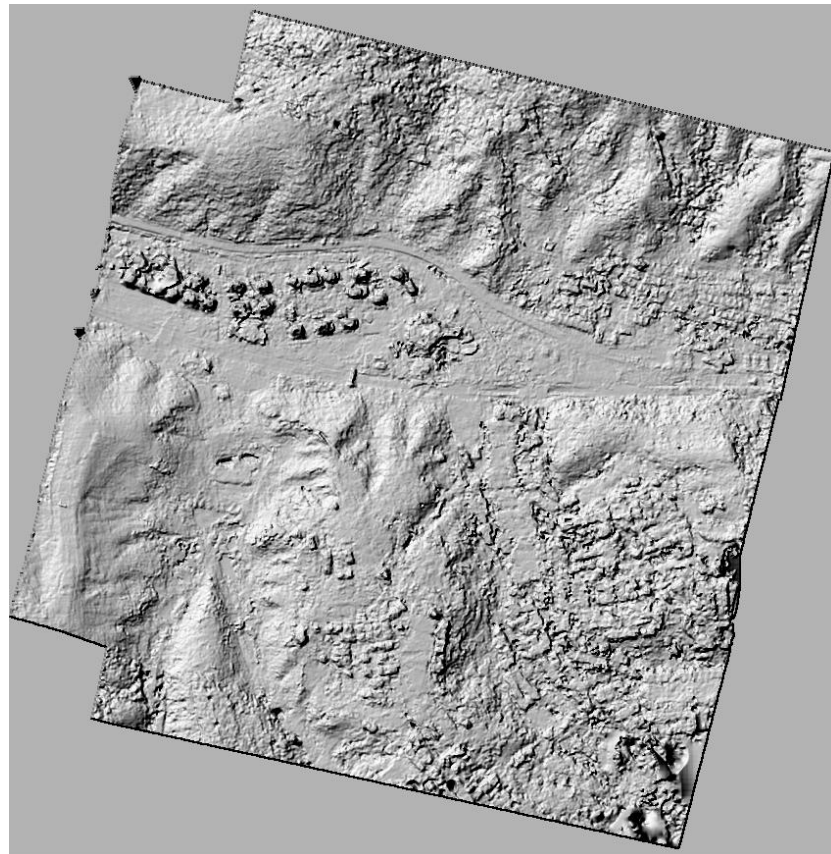


**Figure 4-15: SKS DSM over Ankara Test Site.**
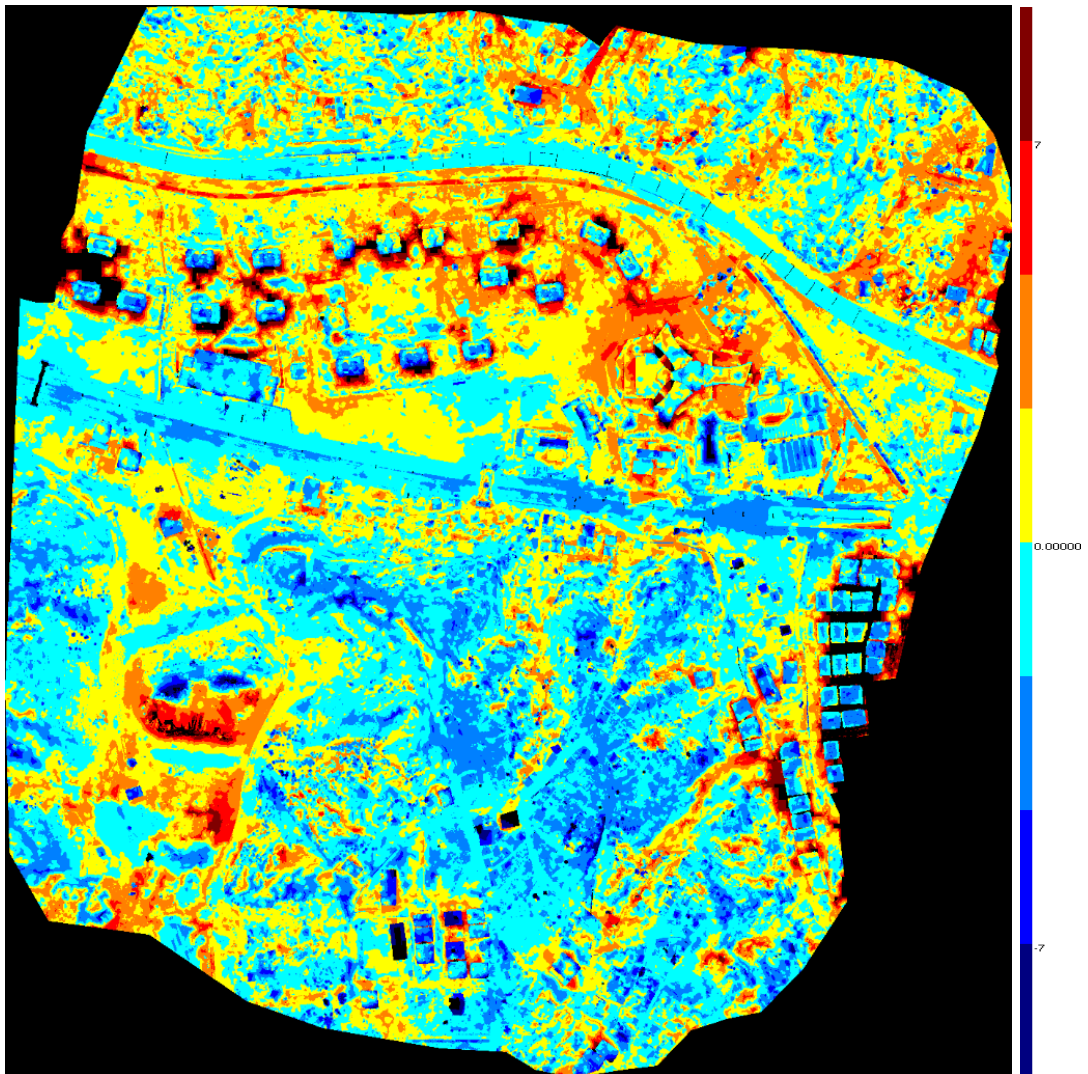
**Figure 4-16: Residuals obtained from the comparison of the SKS DSM with the UAV DSM over Ankara Test Site. The residual errors are in meters.**

The DSM errors are caused by matching errors. These matching errors are mainly due to clouds, shadows, temporal differences between the images, and image artefacts. The matching process might be improved by considering only valid pixels flagged in the related Usable Data Mask, with the condition that UDM information is correct. Examples of the artefacts are shown in Figure 4-17, their name and a short description are recalled just below the relevant image. These artefacts have been report to planet data quality team. For most of them, these are commonly known and well documented in [RD-3] and listed herein [A.3]. Some of these artefacts have been also observed in the EDAP TDS dedicated to visual inspection / Image quality.

| | |
|---|---|
| Due to push broom architecture, these artefacts appear over cloud feature and is located at the limit between two CCDs. | This problem was due to a processing issue, and has been resolved in the last weeks before June 07 2021. |



Anomaly known by the Planet data quality team as « squared processing artefact » is opened, investigations are ongoing.



This is an example of oversharpening and saturation, as well acknowledged and characterised by the Planet data quality team.

**Figure 4-17: Examples to image artefacts observed over Ankara Test Site.**

### 4.7.7  Conclusions

Four critical validation items have been checked for geometric calibration and validation: the absolute accuracy, the temporal accuracy, and the interband registration accuracy and stereoscopic capability. The geometric calibration of SKS 4 and 7 products has been validated for absolute, temporal and interband accuracy. The stereoscopic capability was validated by using the data of SKS 4, 7 and 12.

For all these considered validation items, the results found are in agreement with the accuracy specifications given by the data provider in [RD-3] and the Q3 quality report [RD-5].

**Table 4-16: SKS / EDAP – comparison of Uncertainty Results.**

| | Inter-band Accuracy [m], mean / STD of RMSE | Absolute Accuracy [m], mean / STD of RMSE | Temporal Accuracy [m], mean / STD of RMSE |
|---|---|---|---|
| EDAP Results | Blue-Green: 0.04 / 0.01  Blue - Red: 0.07 / 0.02  Blue -NIR: 0.11 / 0.03 | Scene (Level 1A): 1.45 m / 0.18 m  Ortho (Level 1C_C) 1.14 m / 0.24 m | Ortho (Level 1C_C) 1.51 m / N.A. |
| SKS Q3 quality report [RD-5] | *Blue - Green : 0.11 m / 0.06 m*  *Blue - Red : 0.13 m / 0.08 m*  *Blue - NIR : 0.22 m / 0.14 m* | *3.4 m / 2.6 m* | *3.1 m / 5.7 m* |

The interband accuracy was calculated using six Basic Scene products from two different acquisitions. The absolute accuracy was computed using the Basic Scene and Ortho products from two different acquisitions. The temporal accuracy was obtained from the comparison of the two acquisitions and the RMSE was a single value thus no standard deviation could be calculated. All accuracy values are within the product specifications (1A: < 50 m, 1C: < 10 m). Thus, the geolocation quality is good.

Regarding the stereoscopic capability, no specification was provided by the vendor. The DEM generation and comparison results within EDAP show that the accuracy is related to the temporal differences between the images, image off-nadir configuration, and the improvement of the RPCs using GCPs. The DEM was produced by using three acquisitions of the same area and the compared with the UAV DEM. The global shift between the two DEMs was 0.6 m in height and the standard deviation of the residuals was 2.4 m. These results are in line with the literature (RD-25, RD-27).

The main obstacle in stereoscopic capability was the requirement of RPC improvement using GCPs to be able to produce DEMs. No DEM could be produced prior to RPC improvement. A total of 6 GCPs were used for the improvement of 8 overlapping images from three acquisitions. The main issue was the availability of commercial software for the processing of Basic Scene images and RPCs with 1-3 GCPs, which is often the case for

large-format satellite sensors. The Basic Scene coverage is smaller than most of the linear array imaging sensors, and one RPC file is provided with each scene. The commercial software requires 1-3 GCPs per scene for RPC improvement depending on the selected mathematical model. Since the image sizes are small, the requirement of GCP will be multiplied by the image number used for any DEM production project.

Image quality and the artefacts in the Basic Scene are important for the obtaining quality DEMs. The DEM production is based on the dense image matching, and artefacts such as saturation or repetitive patterns caused by compression or noise lead to false or no matches. Thus, the DEMs in those areas contain gross errors or gaps. Radiometric enhancements such as edge sharpening filters, Wallis filter, noise reduction, etc., would be recommended to improve the DEM quality.

## 4.8    Radiometric Calibration Validation

The assessment proposes to validate SKS family radiometric calibration by using reference data derived from Pseudo Invariant Calibration Site (**PICS**) observations.

### 4.8.1    Activity Description Sheet

<table>
<tr><td colspan="5" align="center"><strong>Radiometric Accuracy Validation</strong></td></tr>
<tr><td colspan="5" align="center"><em>Inputs</em></td></tr>
<tr><td colspan="5">Set of Landsat 8 (OLI)[2], Sentinel-2 (<strong>S2</strong>), MSI, Level 2A data, with atmospheric<br><br>correction applied by using respectively "La Source" and "SMAC".<br><br>Set of Level 1A SKS data (Basic scenes) observed over Libya 4 PICS site (set of products is listed in A.2)</td></tr>
<tr><td colspan="5" align="center"><em>Description</em></td></tr>
<tr><td colspan="5">The scope is to estimate the absolute calibration with in flight method. The accuracy specification claimed by the data provider is within 5%.<br><br>More detailed regarding the radiometric uncertainty values are provided in the Planet Quality Report ([RD-5] Q3 2020 Report). The Planet validation is performed with RadCalNet data considered as reference data source. The absolute radiometric uncertainty results are shown in Table below, as given in ([RD-5].</td></tr>
</table>

| Band | Absolute Accuracy | Precision | Uncertainty (68 Percentile) | Uncertainty (95 Percentile) |
|------|-------------------|-----------|-----------------------------|-----------------------------|
| Blue | 0.0858 | 0.2677 | 0.2811 | 0.5316 |
| Green | 0.1183 | 0.2642 | 0.2895 | 0.5313 |
| Red | 0.0255 | 0.2294 | 0.2308 | 0.4503 |
| NIR | 0.0833 | 0.2368 | 0.2510 | 0.4715 |

<table>
<tr><td colspan="5" align="center"><em>Outputs</em></td></tr>
<tr><td colspan="5">This EDAP assessment validates SKS radiometric calibration by computing absolute calibration ratio for SKS and Sentinel-2 data.<br><br>Considering the family of satellites, the results are in agreement with the radiometric uncertainty results given by the provider. One can note a little disagreement regarding Red band.</td></tr>
</table>

### 4.8.2    Introduction

It was performed an inter comparison exercise with data observed over a PICS site. The reference calibration source is build up with data from Landsat 8 and Sentinel-2 missions. Initially, it was intended to use reference measurements from La Crau RadCalNet. After ordering several images observed at different periods over this geographical location, due to image quality, it has been decided to not use related data.

---

[2] EROS Science Processing Architecture processing (ESPA)

### 4.8.3  Methods and Tools

Calibration site:

PICS sites are referenced by the CEOS (for their utility in radiometric calibration / validation activities. Among PICS, the Libya-4 test site is used. The site is located in the Libyan Desert in Africa at coordinates +28.55° N and +23.39° W, with a terrain elevation of about 118 m above sea level.

The Libya-4 site was first proposed for the Satellite Pour l'Observation de la Terre (SPOT) calibration [RD-17] and demonstrated potential to be utilised for low, medium and high resolution optical visible and near infrared data [RD-18] [RD-19], RD-20], RD-21]. This site is categorised as a "bright" site. As discussed in [RD-22], within the context of reflectance-based methods, this site is characterised by high reflectance in conjunction with low aerosol loading and a predominance of clear skies that reduces the impact of atmospheric errors. Other important aspects are the near Lambertian reflectance, the spectral and spatial uniformity and the temporal stability.

Methodology

The accuracy assessment is performed by comparing between SKS TOA measurements and reference Simulated TOA measurements. As shown in Figure 4-18, simulated TOA measurements (Green Box at the right position in the figure) are derived from temporal Sentinel-2, Landsat 8 Bottom Of Atmosphere (**BOA**) measurements.

There are several processing applied to the reference BOA measurements as:

- Estimate of Bidirectional Reflectance Distribution Function (**BRDF**) model,
- Create spectrum over wavelength interval,
- Estimate corresponding TOA measurement by using the Second Simulation of the Satellite Signal in the Solar Spectrum (6S) Radiative Transfer (RT) code[3],
- Interpolate the TOA spectrum with SKS relative spectral response (spectral convolution).



---

[3] *https://artmotoolbox.com/radiative-transfer-models/89-atmospheric-rtms/27-6sv.html*
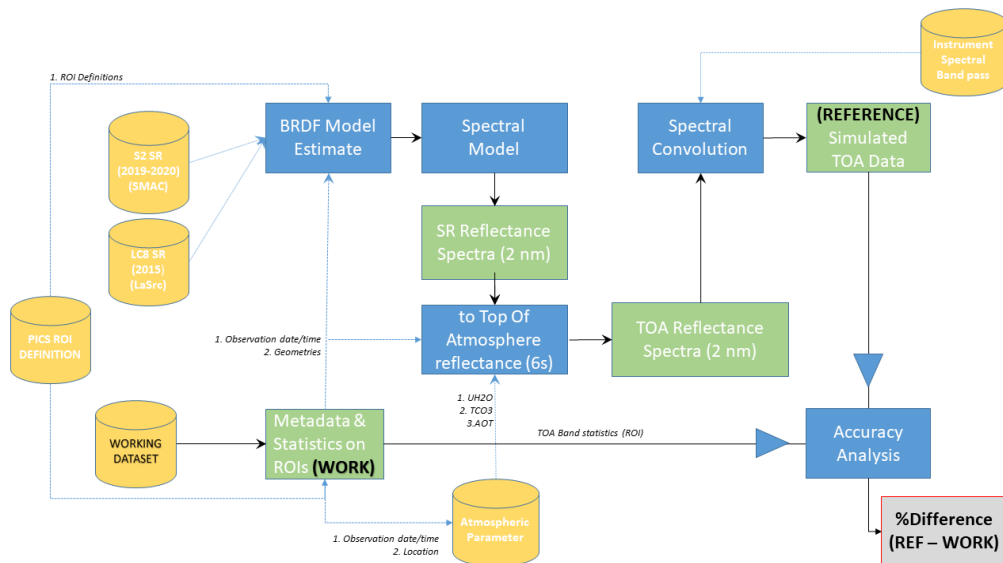
**Figure 4-18: The workflow of absolute radiometric calibration using PICS data.**

Also, the BOA reference spectra is used to simulate TOA reference measurements. The procedure takes into account input observation conditions (geometries of observation) and the sensor properties in particular spectral definition.

The S2 surface reflectance time series, used herein, cover the 2019 / 2020 periods (two years). The MGRS tile code of the Initial BOA products is "34RGS".

Regarding spectral convolution, the SKS RSRs freely available from the planet website are used. As RSR for any SKS missions are proposed, it has been decided, after visual comparison, to always use RSR dataset given for SKS #10 (SKS_RSR_SKS10.csv) instead of considering, depending on the SKS mission, the corresponding RSR dataset.

Finally, the different processing stages are applied sequentially and are broken as follow:

- Create Surface reflectance time series (*S2 BOA TS*) at the ROI locations, three ROIs corresponding to different CCDs have been selected,
- Assessed S2 TS directional effects, output a model and correct data,
- Considering the observation geometry of SKS CCD image, estimate the BOA reflectance for each S2 band,
- Apply spectral interpolation of the BOA reflectance set given at each S2 band central wavelength (*BOA_Spectrum*), with a step of 2 nanometres,
- Considering the observation date, observation geometry (*OBS*), the location of the ROI, collect atmospheric parameters (*ATMS_P*) by using data from Copernicus Atmospheric Monitoring Service (CAMS),
- Use *OBS, ATMS_P* and *BOA_Spectrum* as input of 6S to generate the corresponding *TOA_Spectrum,*
- Collect 3 SKS basic scenes per observation date and per detector, and stitch all the three images for each spectral band
- Extracting at the ROI location, the multi spectral TOA measurements from the SKS stitched images ($TOA\_Measured$)
- Convolved *TOA_Spectrum,* with the SKS spectral response to obtain simulated TOA values at SKS band central wavelength $TOA\_Simulated$
- Computing the calibration ratio, $Q$, and calibration percent difference between simulated and product TOA as follow:

$$\%Difference = \frac{100 * (TOA\_Simulated - TOA\_Measured)}{TOA\_Simulated}$$

Where:

- $TOA\_Measure$ is the measurement processed from the SKS product,
- $TOA\_Simulated$ is the measurement processed from PICS data (S2A).

Image DN is converted to TOA by using coefficients provided directly in the image file header as part of GeoTiff tags. The rescaling coefficients have been validated against results obtained with standard DN to TOA reflectance formula. The in band solar irradiance values (ESUN) are from Table 11 of the Planet user guide (Thuillier spectrum).

As example for one product, the I*mageDescription* GeoTiff Tag provides the following metadata with "*reflectance coefficients*" corresponding to DN to TOA rescaling factors.

```
ImageDescription:    {"properties":    {"radiometric_scale_factor":
"0.01",    "reflectance_coefficients":    [1.8197528559762282e-05,
2.007859131187669e-05, 2.307256162232701e-05, 3.2973493152309087e-
05],   "satellite_azimuth":   100.65639909,   "satellite_elevation":
```

```
72.63397995,    "sun_azimuth":    225.04862152,    "sun_elevation":
60.79583395}}
```

This information (DN to TOA rescaling coefficients) might be stored within JSON metadata.

A representation of Sentinel 2A BOA measurements against scattering angle is shown in Figure 4-19. The linear relationship between scattering angles and BOA measurements is used to estimate expected S2A band BOA values for a given SKS scattering angle.
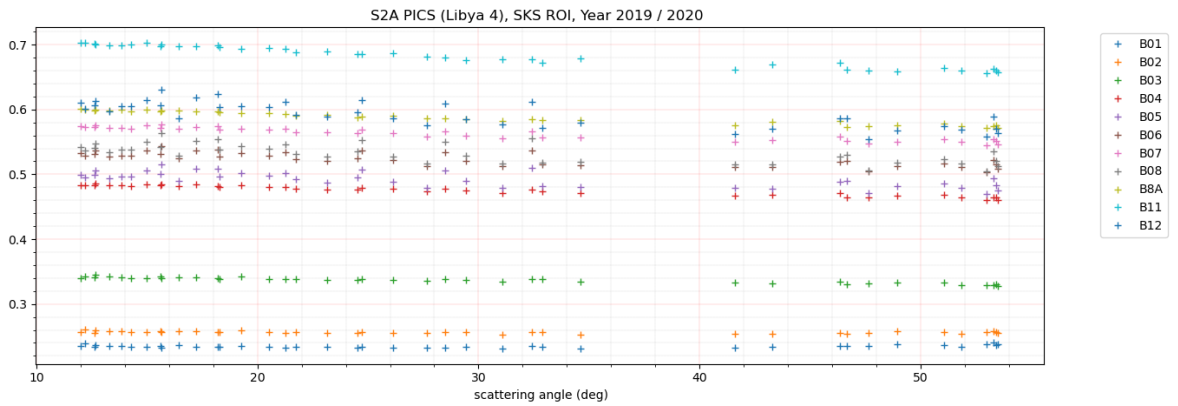


**Figure 4-19: Input to the modelling of bidirectional reflectance distribution function (Sentinel-2A time series).**

Once S2A band BOA values have been selected, a spectral model is applied and SKS TOA values are simulated, as shown in Figure 4-20.
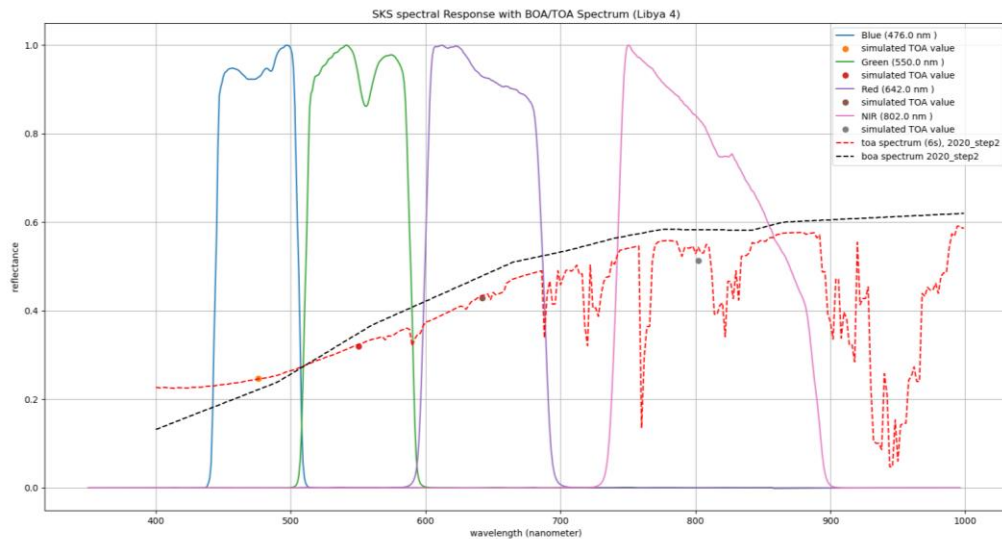


**Figure 4-20: Simulate the top of atmosphere reflectance values at the SKS central wavelength.**

Note that the modelling initially performed with LS8, S2A, S2B shows variability. As the number of S2A products was high (two years of data), it has been decided to keep the same sensor, avoiding to introduce unknown due to inter-calibration, spectral differences.

### 4.8.4  Data

As shown in the Figure 4-21, one set of ROIs have been carefully defined and ROI footprints are in most cases within the SKS CCD image footprints. Note that SKS tile product images are a synthesis of the three CCD images.
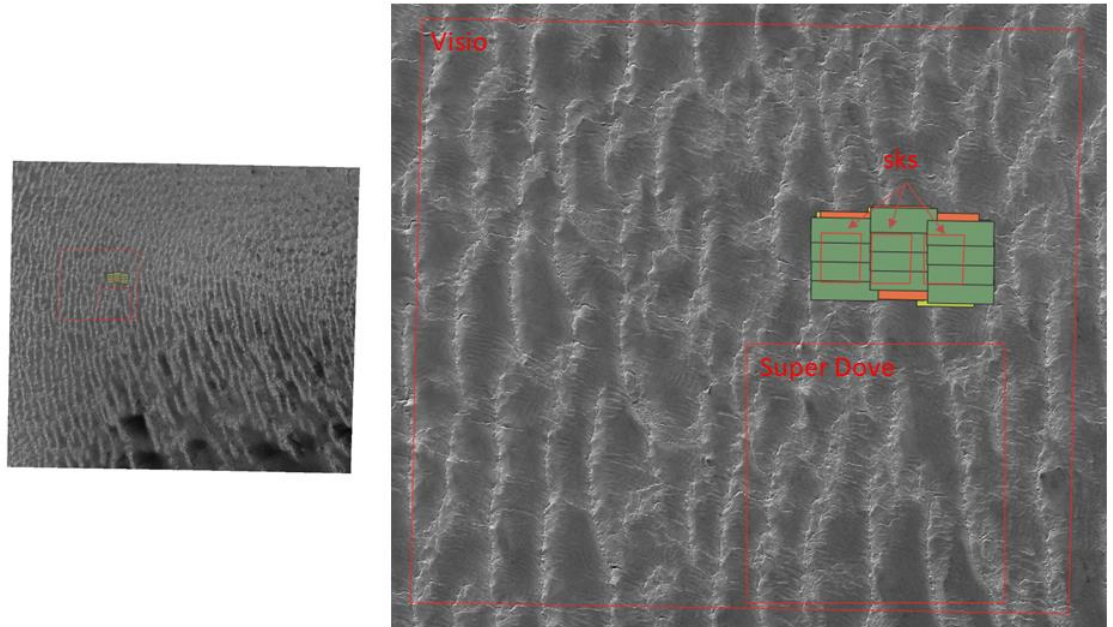


**Figure 4-21: Libya 4 site and region of interest definition, depending on the SKS detector image footprint.**

The Input working data and reference data are described in Appendix.

### 4.8.5  Results

This radiometric calibration validation activity shows that accuracy of SKS family is conformed to the claimed specification: all validation results are within accuracy ranges given by the data provider (< 10%).

As shown in Table 4-17, the EDAP validation shows that accuracy is mainly below 10%. The precision is with 5%, and it is better compared to Planet results (<<28%). These accuracy / precision results leads to an overall uncertainty below 12%.

The main deviations between EDAP and planet team accuracy results are related to the Red band: the EDAP validation outputs 11% whist the Planet validation team outputs 2.5%.

These summary results does not capture the day to day variability that should be more investigated and root causes determined (meteorological or sensor behaviour). Furthermore, as discussed just here after, the EDAP validation results show that for a single date / time, within one image, calibration accuracy of CDDs may strongly differ.

**Table 4-17: Absolute calibration results (PICS), calibration uncertainties.**

| Band | Accuracy | Precision | Uncertainty |
|------|----------|-----------|-------------|
| Blue | 0.1072 | 0.0569 | 0.1214 |
| Green | 0.0818 | 0.0653 | 0.1046 |
| Red | 0.1123 | 0.0455 | 0.1211 |

| | | | |
|---|---|---|---|
| NIR | 0.0970 | 0.0471 | 0.1078 |

Also, the Table 4-18 below list percent difference between simulated TOA measurements and TOA measurements for every product, for every band and for every CCD. The spacecraft identifier is indicated in the column 'Scs', and the CCD is also given.

Taking into account the accuracy of the method (within 5%) and based on a limited number of data, this assessment shows that the radiometric calibration accuracy strongly depends on the concerned SKS mission. Per mission, the results can be summarized as follow:

- Scs 1 calibration is below 5% and whatever the CCD involved
- Scs 7 calibration is temporally stable for CCD "d1" and "d3" and is not stable for CCD "d2"
- Scs 7 calibration is varying depending on the band number for 'd1', from 15% (B1) to 5.5 % (B4)
- Scs 10 calibration is temporally stable, harmonized between CCDs, but above 12% for all bands

More details on input SKS / Simulated values are listed in Table 4-19, Table 4-20.

**Table 4-18: Absolute calibration results (PICS), calibration percent differences.**

| Observation Date | Scs | CCD | B1 | B2 | B3 | B4 |
|---|---|---|---|---|---|---|
| 20200905 | 10 | d3 | 16,61% | 14,51% | 14,67% | 11,42% |
| 20200911 | 1 | d3 | 0,53% | -2,63% | 3,05% | 3,58% |
| 20200917 | 7 | d1 | 13,01% | 8,85% | 10,81% | 5,96% |
| 20200925 | 7 | d1 | 16,66% | 11,01% | 11,34% | 5,40% |
| 20200926 | 10 | d3 | 14,24% | 13,42% | 14,22% | 11,98% |
| 20200905 | 10 | d2 | 15,91% | 14,81% | 16,56% | 14,88% |
| 20200911 | 1 | d2 | 0,34% | -4,18% | 3,60% | 2,34% |
| 20200917 | 7 | d2 | 13,67% | 11,41% | 14,41% | 13,31% |
| 20200925 | 7 | d2 | 8,74% | 7,54% | 9,32% | 7,63% |
| 20200926 | 10 | d2 | 12,45% | 12,11% | 14,64% | 13,34% |
| 20200911 | 1 | d1 | 2,39% | -2,00% | 5,03% | 3,76% |
| 20200917 | 7 | d3 | 11,19% | 7,23% | 10,29% | 12,02% |
| 20200925 | 7 | d3 | 10,51% | 8,42% | 12,70% | 14,83% |
| 20200926 | 10 | d1 | 13,86% | 13,98% | 16,51% | 15,39% |

The measured and simulated TOA measurements (mean value) for every product depending the ROI are listed in table below.

**Table 4-19: Absolute calibration results (PICS), SKS TOA reflectance over ROIs.**

| Observation Date | ROI Id | Scs | CCD | Measure B1 (TOA) | Measure B2 (TOA) | Measure B3 (TOA) | Measure B4 (TOA) |
|---|---|---|---|---|---|---|---|
| 20200905 | 1 | 10 | d3 | 0,21 | 0,27 | 0,36 | 0,44 |
| 20200911 | 1 | 1 | d3 | 0,26 | 0,34 | 0,43 | 0,51 |
| 20200917 | 1 | 7 | d1 | 0,21 | 0,29 | 0,38 | 0,48 |
| 20200925 | 1 | 7 | d1 | 0,21 | 0,28 | 0,38 | 0,48 |
| 20200926 | 1 | 10 | d3 | 0,22 | 0,28 | 0,37 | 0,45 |
| 20200905 | 2 | 10 | d2 | 0,21 | 0,27 | 0,36 | 0,44 |
| 20200911 | 2 | 1 | d2 | 0,26 | 0,35 | 0,43 | 0,52 |
| 20200917 | 2 | 7 | d2 | 0,21 | 0,28 | 0,37 | 0,44 |
| 20200925 | 2 | 7 | d2 | 0,23 | 0,30 | 0,39 | 0,48 |
| 20200926 | 2 | 10 | d2 | 0,23 | 0,29 | 0,37 | 0,45 |
| 20200911 | 3 | 1 | d1 | 0,25 | 0,34 | 0,42 | 0,51 |
| 20200917 | 3 | 7 | d3 | 0,22 | 0,29 | 0,38 | 0,44 |
| 20200925 | 3 | 7 | d3 | 0,22 | 0,29 | 0,37 | 0,44 |
| 20200926 | 3 | 10 | d1 | 0,22 | 0,28 | 0,36 | 0,44 |

**Table 4-20: Absolute calibration results (PICS), Simulated TOA reflectance over ROIs.**

| Observation Date | ROI Id | Scs | CCD | Simulated B1 (TOA) | Simulated B2 (TOA) | Simulated B3 (TOA) | Simulated B4 (TOA) |
|---|---|---|---|---|---|---|---|
| 20200905 | 1 | 10 | d3 | 0,25 | 0,32 | 0,42 | 0,50 |
| 20200911 | 1 | 1 | d3 | 0,26 | 0,33 | 0,44 | 0,53 |
| 20200917 | 1 | 7 | d1 | 0,24 | 0,32 | 0,42 | 0,51 |
| 20200925 | 1 | 7 | d1 | 0,25 | 0,32 | 0,42 | 0,50 |
| 20200926 | 1 | 10 | d3 | 0,26 | 0,33 | 0,43 | 0,51 |
| 20200905 | 2 | 10 | d2 | 0,25 | 0,32 | 0,43 | 0,51 |
| 20200911 | 2 | 1 | d2 | 0,27 | 0,33 | 0,44 | 0,53 |
| 20200917 | 2 | 7 | d2 | 0,25 | 0,32 | 0,43 | 0,51 |
| 20200925 | 2 | 7 | d2 | 0,25 | 0,32 | 0,43 | 0,52 |
| 20200926 | 2 | 10 | d2 | 0,26 | 0,33 | 0,44 | 0,52 |
| 20200911 | 3 | 1 | d1 | 0,26 | 0,33 | 0,44 | 0,53 |
| 20200917 | 3 | 7 | d3 | 0,25 | 0,32 | 0,42 | 0,50 |
| 20200925 | 3 | 7 | d3 | 0,24 | 0,32 | 0,43 | 0,51 |
| 20200926 | 3 | 10 | d1 | 0,26 | 0,32 | 0,43 | 0,51 |

A clear correlation between geometries of observation (Sun, Viewing angles) and calibration results are observed (Table 4-21).

Table 4-21: **Geometries of observation (decimal degree) associated to the input SKS data (mean values).**

| Product Id | Satellite | Observation Geometries | | | |
|---|---|---|---|---|---|
| | | SZA | SAZ | VZA | VAZ |
| 20200905_114616_ssc10d2_0019 | SSC10 | 29,2 | 225 | 16,1 | 100,7 |
| 20200911_091731_ssc1d3_0015 | SSC1 | 28,8 | 144,3 | 23,5 | 100,5 |
| 20200917_115008_ssc7d3_0013 | SSC7 | 34,1 | 222,8 | 9,5 | 99,6 |
| 20200925_115027_ssc7d1_0012 | SSC7 | 37 | 220,7 | 8,7 | 90,9 |
| 20200926_115900_ssc10d3_0014 | SSC10 | 38,6 | 223,2 | 20,9 | 282,7 |

### 4.8.6 Conclusions

This radiometric calibration validation activity shows that accuracy of SKS family is conformed to the claimed specification: all validation results are within accuracy ranges given by the data provider (< 10%). As for SNR assessment, it has been shown that calibration accuracy is good but not consistent within the constellation. It should be confirmed in the future with more dataset and comparison with results from other method (based on RadCalNet data).

# APPENDIX A   MISSION AND PRODUCT

## A.1   Mission Description

The SKS constellation is the VHR component of Planets satellite image portfolio. SKS-A and B generation satellites were launched in 2013/14. The SKS-C generation satellite (60 x 60 x 95 cm) is a high-resolution Earth imaging satellite, first launched in 2016, all collecting thousands of square kilometres of imagery. Each satellite is 3-axis stabilized and agile enough to slew between different targets of interest. Furthermore, each satellite has four thrusters for orbital control, along with four reaction wheels and three magnetic torquers for attitude control. All SKSs contain Cassegrain telescopes with a focal length of 3.6m, with three 5.5 megapixel CMOS imaging detectors making up the focal plane.

Regarding the SKS constellation, the full list of satellite is given in[4] and report herein in Table 22: List of SKS Satellites.

Imagery are captured in a continuous strip of single frame images known as "scenes", which are all acquired in the blue, green, red, NIR-infrared, and panchromatic bands, with following spectral bandwidth definition:

- Blue: 455 - 515 nm,
- Green: 500 - 590 nm,
- Red: 590 - 670 nm,
- NIR: 780 - 860 nm,
- Panchromatic band: 450-900 nm.

The RSR curves of SKS #10 are shown in Figure 4-20 and compared with Sentinel-2 MSI ones. Furthermore, the atmospheric transmittance curve (obtained with 6S) is added in background. The spectral bandwidth of SKS RSRs is larger than Sentinel-2 ones. More over respective NIR central wavelength values (not shown in the figure) are shifted. Because both SKS, Sentinel-2 RSRs are of different shapes and localization of H20 absorption bands (NIR), the use of the proposed EDAP calibration approach (Section 4.8) is fully justified.

The ground sampling distance depends on the spectral channel and on the image mode. Latest products are observed with PBHDR is imaging mode. The PBHDR mode actually changes the capture settings of the spacecraft and the camera. It is not a processing method but an acquisition method. It is a way to artificially reduce the scan rate by vibrating the camera in synchronisation with the spacecraft velocity and frame rate. It allows to increase the SNR while also increasing the capacity of each spacecraft.

---

[4] https://space.skyrocket.de/doc_sdat/SKS-3.htm (Visited in January 5, 2021)
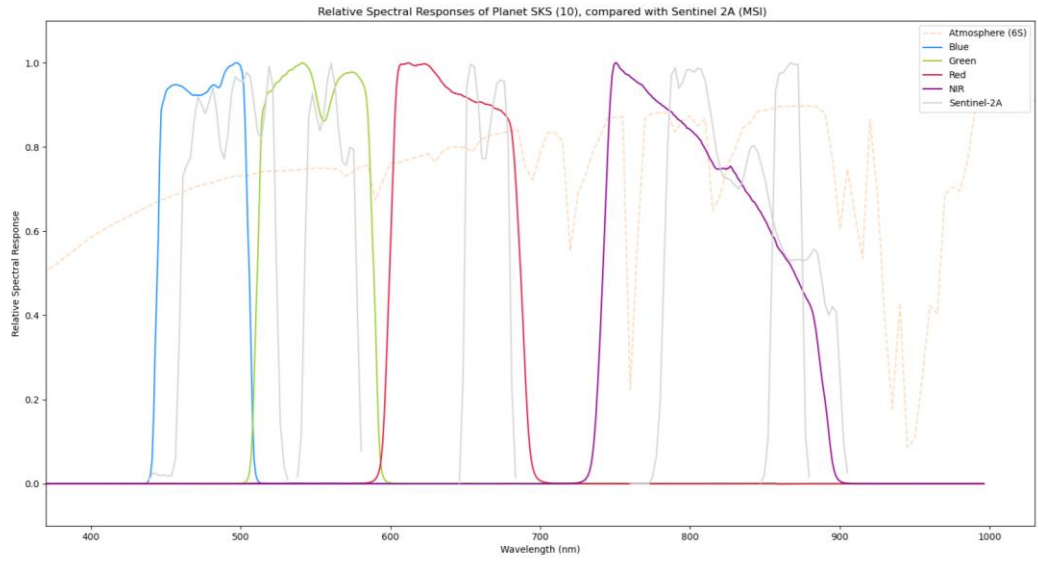
**Figure 4-22: Comparison of SKS and Sentinel-2 RSRs together with atmospheric transmittance (6s) over a wavelength interval within 350 nm, 1000 nm interval.**

**Table 22: List of SKS Satellites.**

| Satellite | COSPAR | Date | LS | Launch Vehicle | Remarks |
|---|---|---|---|---|---|
| SkySat 3 (SkySat C1) | 2016-040C | 22.06.2016 | Sr SLP | PSLV-XL | with Cartosat 2C, BIROS, M3MSat, LAPAN A3, GHGSat D, Flock-2p 1, ..., 12, SathyabamaSat, Swayam, BeeSat 4 |
| SkySat 4 (SkySat C2) | 2016-058D | 16.09.2016 | Ko ELV | Vega | with PerúSat 1, SkySat 5, SkySat 6, SkySat 7 |
| SkySat 5 (SkySat C3) | 2016-058E | 16.09.2016 | Ko ELV | Vega | with PerúSat 1, SkySat 4, SkySat 6, SkySat 7 |
| SkySat 6 (SkySat C4) | 2016-058B | 16.09.2016 | Ko ELV | Vega | with PerúSat 1, SkySat 4, SkySat 5, SkySat 7 |
| SkySat 7 (SkySat C5) | 2016-058C | 16.09.2016 | Ko ELV | Vega | with PerúSat 1, SkySat 4, SkySat 5, SkySat 6 |
| SkySat 8 (SkySat C6) | 2017-068F | 31.10.2017 | Va 576E | Minotaur-C-XL-3210 | with SkySat 9, SkySat 10, SkySat 11, SkySat 12, SkySat 13, Flock-3m 1, ..., 4 |
| SkySat 9 (SkySat C7) | 2017-068E | 31.10.2017 | Va 576E | Minotaur-C-XL-3210 | with SkySat 8, SkySat 10, SkySat 11, SkySat 12, SkySat 13, Flock-3m 1, ..., 4 |
| SkySat 10 (SkySat C8) | 2017-068D | 31.10.2017 | Va 576E | Minotaur-C-XL-3210 | with SkySat 8, SkySat 9, SkySat 11, SkySat 12, SkySat 13, Flock-3m 1, ..., 4 |
| SkySat 11 (SkySat C9) | 2017-068C | 31.10.2017 | Va 576E | Minotaur-C-XL-3210 | with SkySat 8, SkySat 9, SkySat 10, SkySat 12, SkySat 13, Flock-3m 1, ..., 4 |
| SkySat 12 (SkySat C10) | 2017-068B | 31.10.2017 | Va 576E | Minotaur-C-XL-3210 | with SkySat 8, SkySat 9, SkySat 10, SkySat 11, SkySat 13, Flock-3m 1, ..., 4 |
| SkySat 13 (SkySat C11) | 2017-068A | 31.10.2017 | Va 576E | Minotaur-C-XL-3210 | with SkySat 8, SkySat 9, SkySat 10, SkySat 11, SkySat 12, Flock-3m 1, ..., 4 |
| SkySat 14 (SkySat C12) | 2018-099AR | 03.12.2018 | Va SLC-4E | Falcon-9 v1.2 (Block 5) | with SkySat 15, Eu:CROPIS, STPSat 5, FalconSat 6, NEXTSat 1, KazSTSAT, eXCITe, SeeMe, ICEYE X2, BlackSky Global 2, ESEO, Hawk A, B, C, Capella 1, AISTECHSAT 2, CSIM-FD, Hiber 2, ITASAT 1, Landmapper-BC 4, ORS 7A, 7B, Al-Farabi 2, Astrocast 0.1, Audacy 0, BRIO, Centauri 1, Eaglet 1, Enoch, Flock-3s 1, 2, 3, K2SAT, KazSciSat 1, MinXSS 2, Orbital Reflector, RAAF M1, SeaHawk 1, SNUSAT 2, THEA, VESTA, PW-Sat 2, SNUGLITE, VisionCube, RANGE A, B, Elysium-Star 2, ExseedSat 1, Fox 1C, Irvine 02, JY1-Sat, KNACKSAT, MOVE 2, SpaceBEE 5, 6, 7, Suomi-100, WeissSat 1, Sirion Pathfinder 2, OrbWeaver 1, 2, SPAWAR-CAL 0, OR, R |
| SkySat 15 (SkySat C13) | 2018-099AW | 03.12.2018 | Va SLC-4E | Falcon-9 v1.2 (Block 5) | with SkySat 14, Eu:CROPIS, STPSat 5, FalconSat 6, NEXTSat 1, KazSTSAT, eXCITe, SeeMe, ICEYE X2, BlackSky Global 2, ESEO, Hawk A, B, C, Capella 1, AISTECHSAT 2, CSIM-FD, Hiber 2, ITASAT 1, Landmapper-BC 4, ORS 7A, 7B, Al-Farabi 2, Astrocast 0.1, Audacy 0, BRIO, Centauri 1, Eaglet 1, Enoch, Flock-3s 1, 2, 3, K2SAT, KazSciSat 1, MinXSS 2, Orbital Reflector, |

| | | | | | RAAF M1, SeaHawk 1, SNUSAT 2, THEA, VESTA, PW-Sat 2, SNUGLITE, VisionCube, RANGE A, B, Elysium-Star 2, ExseedSat 1, Fox 1C, Irvine 02, JY1-Sat, KNACKSAT, MOVE 2, SpaceBEE 5, 6, 7, Suomi-100, WeissSat 1, Sirion Pathfinder 2, OrbWeaver 1, 2, SPAWAR-CAL 0, OR, R |
|---|---|---|---|---|---|
| SkySat 16 (SkySat C14) | 2020-038BL | 13.06.2020 | CC SLC-40 | Falcon-9 v1.2 (Block 5) | with Starlink v1.0 8-1, ..., 8-58, SkySat 17, SkySat 18 |
| SkySat 17 (SkySat C15) | 2020-038BM | 13.06.2020 | CC SLC-40 | Falcon-9 v1.2 (Block 5) | with Starlink v1.0 8-1, ..., 8-58, SkySat 16, SkySat 18 |
| SkySat 18 (SkySat C16) | 2020-038BN | 13.06.2020 | CC SLC-40 | Falcon-9 v1.2 (Block 5) | with Starlink v1.0 8-1, ..., 8-58, SkySat 16, SkySat 17 |
| SkySat 19 (SkySat C17) | 2020-057BQ | 18.08.2020 | CC SLC-40 | Falcon-9 v1.2 (Block 5) | with Starlink v1.0 10-1, ..., 10-58, SkySat 20, SkySat 21 |
| SkySat 20 (SkySat C18) | 2020-057BR | 18.08.2020 | CC SLC-40 | Falcon-9 v1.2 (Block 5) | with Starlink v1.0 10-1, ..., 10-58, SkySat 19, SkySat 21 |
| SkySat 21 (SkySat C19) | 2020-057BS | 18.08.2020 | CC SLC-40 | Falcon-9 v1.2 (Block 5) | with Starlink v1.0 10-1, ..., 10-58, SkySat 19, SkySat 20 |

## A.2   Test Data Set

Two distinct methods have been used to select and collect the SKS Test Data Set (TDS); the first one by using the Planet Catalog (Level 3B), and the second through the API (Level 1B)

The TDS used is listed below depending on the validation items.

**Image Quality TDS (4.4, 4.5,4.6)**

Address all Image quality aspects, including product format, quality mask and image visual inspection. Furthermore, dataset have been collected over MTF artificial targets. Libya 4 dataset has been used to assess SNR Quality parameters, so please refer to corresponding sub-section below (Radiometric Calibration TDS).

**SKS Scene Products:**

- o   20210314_101355_ssc4_u0001_pansharpened (SALON POI)
- o   20201229_112916_ssc17d2_0018_basic_analytic (SALON MTF)
- o   20190426_061329_ssc6d2_0003_basic_analytic (BAOUTOU MTF)
- o   20200429_033013_ssc13d2_0015_basic_analytic (BAOUTOU MTF)

**Reference Products:**

Pleiades HR Data for comparison with Pansharpened products (ESA TPM CAT-One 63602):

- •   SO21041658-2-
  01_DS_PHR1B_201409251042136_FR1_PX_E005N43_0215_01048

**Geometric Calibration Validation TDS (4.7)**

**SKS Collect Ortho Products:**

- o   20200718_082806_ssc4_u0001_analytic
- o   20200718_082806_ssc4_u0002_analytic
- o   20200923_112354_ssc7_u0001_analytic
- o   20200923_112354_ssc7_u0002_analytic

**SKS Scene Products:**

- o   20200718_082806_ssc4d1_0008_basic_panchromatic
- o   20200718_082806_ssc4d1_0009_basic_panchromatic
- o   20200718_082806_ssc4d1_0010_basic_panchromatic
- o   20200718_082806_ssc4d1_0011_basic_panchromatic
- o   20200718_082806_ssc4d1_0012_basic_panchromatic
- o   20200718_082806_ssc4d1_0013_basic_panchromatic
- o   20200718_082806_ssc4d1_0014_basic_panchromatic
- o   20200718_082806_ssc4d1_0015_basic_panchromatic
- o   20200718_082806_ssc4d1_0016_basic_panchromatic
- o   20200718_082806_ssc4d1_0017_basic_panchromatic
- o   20200718_082806_ssc4d1_0018_basic_panchromatic
- o   20200718_082806_ssc4d1_0019_basic_panchromatic
- o   20200718_082806_ssc4d1_0020_basic_panchromatic
- o   20200718_082806_ssc4d1_0021_basic_panchromatic
- o   20200718_082806_ssc4d1_0022_basic_panchromatic

- o 20200718_082806_ssc4d1_0023_basic_panchromatic
- o 20200718_082806_ssc4d1_0024_basic_panchromatic
- o 20200718_082806_ssc4d1_0025_basic_panchromatic
- o 20200718_082806_ssc4d1_0026_basic_panchromatic
- o 20200718_082806_ssc4d2_0013_basic_panchromatic
- o 20200718_082806_ssc4d2_0014_basic_panchromatic
- o 20200718_082806_ssc4d2_0015_basic_panchromatic
- o 20200718_082806_ssc4d2_0016_basic_panchromatic
- o 20200718_082806_ssc4d2_0017_basic_panchromatic
- o 20200718_082806_ssc4d2_0018_basic_panchromatic
- o 20200718_082806_ssc4d2_0019_basic_panchromatic
- o 20200718_082806_ssc4d2_0020_basic_panchromatic
- o 20200718_082806_ssc4d2_0021_basic_panchromatic

- o 20200718_082806_ssc4d2_0022_basic_panchromatic
- o 20200718_082806_ssc4d2_0023_basic_panchromatic
- o 20200718_082806_ssc4d2_0024_basic_panchromatic
- o 20200718_082806_ssc4d2_0025_basic_panchromatic
- o 20200718_082806_ssc4d2_0026_basic_panchromatic
- o 20200718_082806_ssc4d2_0027_basic_panchromatic
- o 20200718_082806_ssc4d2_0028_basic_panchromatic
- o 20200718_082806_ssc4d2_0029_basic_panchromatic
- o 20200718_082806_ssc4d2_0030_basic_panchromatic
- o 20200718_082806_ssc4d2_0031_basic_panchromatic
- o 20200718_082806_ssc4d3_0009_basic_panchromatic
- o 20200718_082806_ssc4d3_0010_basic_panchromatic
- o 20200718_082806_ssc4d3_0011_basic_panchromatic
- o 20200718_082806_ssc4d3_0012_basic_panchromatic
- o 20200718_082806_ssc4d3_0013_basic_panchromatic
- o 20200718_082806_ssc4d3_0014_basic_panchromatic
- o 20200718_082806_ssc4d3_0015_basic_panchromatic
- o 20200718_082806_ssc4d3_0016_basic_panchromatic
- o 20200718_082806_ssc4d3_0017_basic_panchromatic
- o 20200718_082806_ssc4d3_0018_basic_panchromatic
- o 20200718_082806_ssc4d3_0019_basic_panchromatic
- o 20200718_082806_ssc4d3_0020_basic_panchromatic
- o 20200718_082806_ssc4d3_0021_basic_panchromatic
- o 20200718_082806_ssc4d3_0022_basic_panchromatic
- o 20200718_082806_ssc4d3_0023_basic_panchromatic
- o 20200718_082806_ssc4d3_0024_basic_panchromatic
- o 20200718_082806_ssc4d3_0025_basic_panchromatic
- o 20200718_082806_ssc4d3_0026_basic_panchromatic
- o 20200718_082806_ssc4d3_0027_basic_panchromatic
- o 20200718_082806_ssc4d3_0028_basic_panchromatic

- o 20200923_112354_ssc7d1_0012_basic_panchromatic
- o 20200923_112354_ssc7d1_0013_basic_panchromatic
- o 20200923_112354_ssc7d1_0014_basic_panchromatic
- o 20200923_112354_ssc7d1_0015_basic_panchromatic
- o 20200923_112354_ssc7d1_0016_basic_panchromatic
- o 20200923_112354_ssc7d1_0017_basic_panchromatic
- o 20200923_112354_ssc7d1_0018_basic_panchromatic
- o 20200923_112354_ssc7d1_0019_basic_panchromatic
- o 20200923_112354_ssc7d1_0020_basic_panchromatic
- o 20200923_112354_ssc7d1_0021_basic_panchromatic
- o 20200923_112354_ssc7d1_0022_basic_panchromatic
- o 20200923_112354_ssc7d1_0023_basic_panchromatic
- o 20200923_112354_ssc7d1_0024_basic_panchromatic

- 20200923_112354_ssc7d1_0025_basic_panchromatic
- 20200923_112354_ssc7d1_0026_basic_panchromatic
- 20200923_112354_ssc7d1_0027_basic_panchromatic
- 20200923_112354_ssc7d1_0028_basic_panchromatic
- 20200923_112354_ssc7d1_0029_basic_panchromatic
- 20200923_112354_ssc7d1_0030_basic_panchromatic
- 20200923_112354_ssc7d1_0031_basic_panchromatic
- 20200923_112354_ssc7d1_0032_basic_panchromatic
- 20200923_112354_ssc7d2_0016_basic_panchromatic
- 20200923_112354_ssc7d2_0017_basic_panchromatic
- 20200923_112354_ssc7d2_0018_basic_panchromatic
- 20200923_112354_ssc7d2_0019_basic_panchromatic
- 20200923_112354_ssc7d2_0020_basic_panchromatic
- 20200923_112354_ssc7d2_0021_basic_panchromatic

- 20200923_112354_ssc7d2_0022_basic_panchromatic
- 20200923_112354_ssc7d2_0023_basic_panchromatic
- 20200923_112354_ssc7d2_0024_basic_panchromatic
- 20200923_112354_ssc7d2_0025_basic_panchromatic
- 20200923_112354_ssc7d2_0026_basic_panchromatic
- 20200923_112354_ssc7d2_0027_basic_panchromatic
- 20200923_112354_ssc7d2_0028_basic_panchromatic
- 20200923_112354_ssc7d2_0029_basic_panchromatic
- 20200923_112354_ssc7d2_0030_basic_panchromatic
- 20200923_112354_ssc7d2_0031_basic_panchromatic
- 20200923_112354_ssc7d2_0032_basic_panchromatic
- 20200923_112354_ssc7d2_0033_basic_panchromatic
- 20200923_112354_ssc7d2_0034_basic_panchromatic
- 20200923_112354_ssc7d2_0035_basic_panchromatic
- 20200923_112354_ssc7d2_0036_basic_panchromatic
- 20200923_112354_ssc7d3_0012_basic_panchromatic
- 20200923_112354_ssc7d3_0013_basic_panchromatic
- 20200923_112354_ssc7d3_0014_basic_panchromatic
- 20200923_112354_ssc7d3_0015_basic_panchromatic
- 20200923_112354_ssc7d3_0016_basic_panchromatic
- 20200923_112354_ssc7d3_0017_basic_panchromatic
- 20200923_112354_ssc7d3_0018_basic_panchromatic
- 20200923_112354_ssc7d3_0019_basic_panchromatic
- 20200923_112354_ssc7d3_0020_basic_panchromatic
- 20200923_112354_ssc7d3_0021_basic_panchromatic
- 20200923_112354_ssc7d3_0022_basic_panchromatic
- 20200923_112354_ssc7d3_0023_basic_panchromatic
- 20200923_112354_ssc7d3_0024_basic_panchromatic
- 20200923_112354_ssc7d3_0025_basic_panchromatic
- 20200923_112354_ssc7d3_0026_basic_panchromatic
- 20200923_112354_ssc7d3_0027_basic_panchromatic
- 20200923_112354_ssc7d3_0028_basic_panchromatic
- 20200923_112354_ssc7d3_0029_basic_panchromatic
- 20200923_112354_ssc7d3_0030_basic_panchromatic
- 20200923_112354_ssc7d3_0031_basic_panchromatic
- 20200923_112354_ssc7d3_0032_basic_panchromatic
- 20200923_112354_ssc7d3_0033_basic_panchromatic

- 20200927_083429_ssc12d3_0022_basic_panchromatic
- 20200927_083429_ssc12d3_0023_basic_panchromatic
- 20200927_083429_ssc12d3_0024_basic_panchromatic

20200718_082806_ssc4d1_0008_basic_analytic
20200718_082806_ssc4d1_0009_basic_analytic
20200718_082806_ssc4d1_0010_basic_analytic
20200718_082806_ssc4d1_0011_basic_analytic
20200718_082806_ssc4d1_0012_basic_analytic
20200718_082806_ssc4d1_0013_basic_analytic
20200718_082806_ssc4d1_0014_basic_analytic
20200718_082806_ssc4d1_0015_basic_analytic
20200718_082806_ssc4d1_0016_basic_analytic
20200718_082806_ssc4d1_0017_basic_analytic
20200718_082806_ssc4d1_0018_basic_analytic
20200718_082806_ssc4d1_0019_basic_analytic
20200718_082806_ssc4d1_0020_basic_analytic
20200718_082806_ssc4d1_0021_basic_analytic
20200718_082806_ssc4d1_0022_basic_analytic
20200718_082806_ssc4d1_0023_basic_analytic
20200718_082806_ssc4d1_0024_basic_analytic
20200718_082806_ssc4d1_0025_basic_analytic
20200718_082806_ssc4d1_0026_basic_analytic
20200718_082806_ssc4d2_0013_basic_analytic
20200718_082806_ssc4d2_0014_basic_analytic
20200718_082806_ssc4d2_0015_basic_analytic
20200718_082806_ssc4d2_0016_basic_analytic
20200718_082806_ssc4d2_0017_basic_analytic
20200718_082806_ssc4d2_0018_basic_analytic
20200718_082806_ssc4d2_0019_basic_analytic
20200718_082806_ssc4d2_0020_basic_analytic
20200718_082806_ssc4d2_0021_basic_analytic
20200718_082806_ssc4d2_0022_basic_analytic
20200718_082806_ssc4d2_0023_basic_analytic
20200718_082806_ssc4d2_0024_basic_analytic
20200718_082806_ssc4d2_0025_basic_analytic
20200718_082806_ssc4d2_0026_basic_analytic
20200718_082806_ssc4d2_0027_basic_analytic
20200718_082806_ssc4d2_0028_basic_analytic
20200718_082806_ssc4d2_0029_basic_analytic
20200718_082806_ssc4d2_0030_basic_analytic
20200718_082806_ssc4d2_0031_basic_analytic
20200718_082806_ssc4d3_0009_basic_analytic
20200718_082806_ssc4d3_0010_basic_analytic
20200718_082806_ssc4d3_0011_basic_analytic
20200718_082806_ssc4d3_0012_basic_analytic
20200718_082806_ssc4d3_0013_basic_analytic
20200718_082806_ssc4d3_0014_basic_analytic
20200718_082806_ssc4d3_0015_basic_analytic
20200718_082806_ssc4d3_0016_basic_analytic
20200718_082806_ssc4d3_0017_basic_analytic
20200718_082806_ssc4d3_0018_basic_analytic
20200718_082806_ssc4d3_0019_basic_analytic
20200718_082806_ssc4d3_0020_basic_analytic
20200718_082806_ssc4d3_0021_basic_analytic
20200718_082806_ssc4d3_0022_basic_analytic
20200718_082806_ssc4d3_0023_basic_analytic
20200718_082806_ssc4d3_0024_basic_analytic
20200718_082806_ssc4d3_0025_basic_analytic
20200718_082806_ssc4d3_0026_basic_analytic
20200718_082806_ssc4d3_0027_basic_analytic

20200718_082806_ssc4d3_0028_basic_analytic

20200923_112354_ssc7d1_0012_basic_analytic
20200923_112354_ssc7d1_0012_basic_analytic
20200923_112354_ssc7d1_0013_basic_analytic
20200923_112354_ssc7d1_0014_basic_analytic
20200923_112354_ssc7d1_0015_basic_analytic
20200923_112354_ssc7d1_0016_basic_analytic
20200923_112354_ssc7d1_0017_basic_analytic
20200923_112354_ssc7d1_0018_basic_analytic
20200923_112354_ssc7d1_0019_basic_analytic
20200923_112354_ssc7d1_0020_basic_analytic
20200923_112354_ssc7d1_0021_basic_analytic
20200923_112354_ssc7d1_0022_basic_analytic
20200923_112354_ssc7d1_0023_basic_analytic
20200923_112354_ssc7d1_0024_basic_analytic
20200923_112354_ssc7d1_0025_basic_analytic
20200923_112354_ssc7d1_0026_basic_analytic
20200923_112354_ssc7d1_0027_basic_analytic
20200923_112354_ssc7d1_0028_basic_analytic
20200923_112354_ssc7d1_0029_basic_analytic
20200923_112354_ssc7d1_0030_basic_analytic
20200923_112354_ssc7d1_0031_basic_analytic
20200923_112354_ssc7d1_0032_basic_analytic
20200923_112354_ssc7d2_0016_basic_analytic
20200923_112354_ssc7d2_0017_basic_analytic
20200923_112354_ssc7d2_0018_basic_analytic
20200923_112354_ssc7d2_0019_basic_analytic
20200923_112354_ssc7d2_0020_basic_analytic
20200923_112354_ssc7d2_0021_basic_analytic
20200923_112354_ssc7d2_0022_basic_analytic
20200923_112354_ssc7d2_0023_basic_analytic
20200923_112354_ssc7d2_0024_basic_analytic
20200923_112354_ssc7d2_0025_basic_analytic
20200923_112354_ssc7d2_0026_basic_analytic
20200923_112354_ssc7d2_0027_basic_analytic
20200923_112354_ssc7d2_0028_basic_analytic
20200923_112354_ssc7d2_0029_basic_analytic
20200923_112354_ssc7d2_0030_basic_analytic
20200923_112354_ssc7d2_0031_basic_analytic
20200923_112354_ssc7d2_0032_basic_analytic
20200923_112354_ssc7d2_0033_basic_analytic
20200923_112354_ssc7d2_0034_basic_analytic
20200923_112354_ssc7d2_0035_basic_analytic
20200923_112354_ssc7d2_0036_basic_analytic
20200923_112354_ssc7d3_0012_basic_analytic
20200923_112354_ssc7d3_0013_basic_analytic
20200923_112354_ssc7d3_0014_basic_analytic
20200923_112354_ssc7d3_0015_basic_analytic
20200923_112354_ssc7d3_0016_basic_analytic
20200923_112354_ssc7d3_0017_basic_analytic
20200923_112354_ssc7d3_0018_basic_analytic
20200923_112354_ssc7d3_0019_basic_analytic
20200923_112354_ssc7d3_0020_basic_analytic
20200923_112354_ssc7d3_0021_basic_analytic
20200923_112354_ssc7d3_0022_basic_analytic
20200923_112354_ssc7d3_0023_basic_analytic
20200923_112354_ssc7d3_0024_basic_analytic

20200923_112354_ssc7d3_0025_basic_analytic
20200923_112354_ssc7d3_0026_basic_analytic
20200923_112354_ssc7d3_0027_basic_analytic
20200923_112354_ssc7d3_0028_basic_analytic
20200923_112354_ssc7d3_0029_basic_analytic
20200923_112354_ssc7d3_0030_basic_analytic
20200923_112354_ssc7d3_0031_basic_analytic
20200923_112354_ssc7d3_0032_basic_analytic
20200923_112354_ssc7d3_0033_basic_analytic

Radiometric Calibration TDS (4.8)

Ortho scenes (Level 1C) data have been used for radiometric calibration. Images have been selected depending on camera used for data acquisition. The objective was to fully overlap the extent of the shape files defined per detector as explained in the related document section.

- o 20200905_114616_ssc10d2_0019_basic_analytic
- o 20200905_114616_ssc10d3_0014_basic_analytic
- o 20200905_114616_ssc10d3_0015_basic_analytic
- o 20200911_091731_ssc1d1_0013_basic_analytic
- o 20200911_091731_ssc1d1_0014_basic_analytic
- o 20200911_091731_ssc1d1_0015_basic_analytic
- o 20200911_091731_ssc1d1_0016_basic_analytic
- o 20200911_091731_ssc1d2_0016_basic_analytic
- o 20200911_091731_ssc1d2_0017_basic_analytic
- o 20200911_091731_ssc1d2_0018_basic_analytic
- o 20200911_091731_ssc1d2_0019_basic_analytic
- o 20200911_091731_ssc1d3_0013_basic_analytic
- o 20200911_091731_ssc1d3_0014_basic_analytic
- o 20200911_091731_ssc1d3_0015_basic_analytic
- o 20200911_091731_ssc1d3_0016_basic_analytic
- o 20200917_115008_ssc7d1_0012_basic_analytic
- o 20200917_115008_ssc7d1_0013_basic_analytic
- o 20200917_115008_ssc7d1_0014_basic_analytic
- o 20200917_115008_ssc7d1_0015_basic_analytic
- o 20200917_115008_ssc7d2_0008_basic_analytic
- o 20200917_115008_ssc7d2_0009_basic_analytic
- o 20200917_115008_ssc7d2_0010_basic_analytic
- o 20200917_115008_ssc7d2_0011_basic_analytic
- o 20200917_115008_ssc7d2_0012_basic_analytic
- o 20200917_115008_ssc7d3_0012_basic_analytic
- o 20200917_115008_ssc7d3_0013_basic_analytic
- o 20200917_115008_ssc7d3_0014_basic_analytic
- o 20200917_115008_ssc7d3_0015_basic_analytic
- o 20200925_115027_ssc7d1_0012_basic_analytic
- o 20200925_115027_ssc7d1_0013_basic_analytic
- o 20200925_115027_ssc7d1_0014_basic_analytic
- o 20200925_115027_ssc7d1_0015_basic_analytic
- o 20200925_115027_ssc7d2_0008_basic_analytic
- o 20200925_115027_ssc7d2_0009_basic_analytic
- o 20200925_115027_ssc7d2_0010_basic_analytic
- o 20200925_115027_ssc7d2_0011_basic_analytic
- o 20200925_115027_ssc7d2_0012_basic_analytic
- o 20200925_115027_ssc7d3_0012_basic_analytic
- o 20200925_115027_ssc7d3_0013_basic_analytic

- o 20200925_115027_ssc7d3_0014_basic_analytic
- o 20200925_115027_ssc7d3_0015_basic_analytic
- o 20200925_115027_ssc7d3_0016_basic_analytic
- o 20200926_115900_ssc10d1_0013_basic_analytic
- o 20200926_115900_ssc10d1_0014_basic_analytic
- o 20200926_115900_ssc10d1_0015_basic_analytic
- o 20200926_115900_ssc10d1_0016_basic_analytic
- o 20200926_115900_ssc10d2_0017_basic_analytic
- o 20200926_115900_ssc10d2_0018_basic_analytic
- o 20200926_115900_ssc10d2_0019_basic_analytic
- o 20200926_115900_ssc10d3_0013_basic_analytic
- o 20200926_115900_ssc10d3_0014_basic_analytic
- o 20200926_115900_ssc10d3_0015_basic_analytic
- o 20200926_115900_ssc10d3_0016_basic_analytic
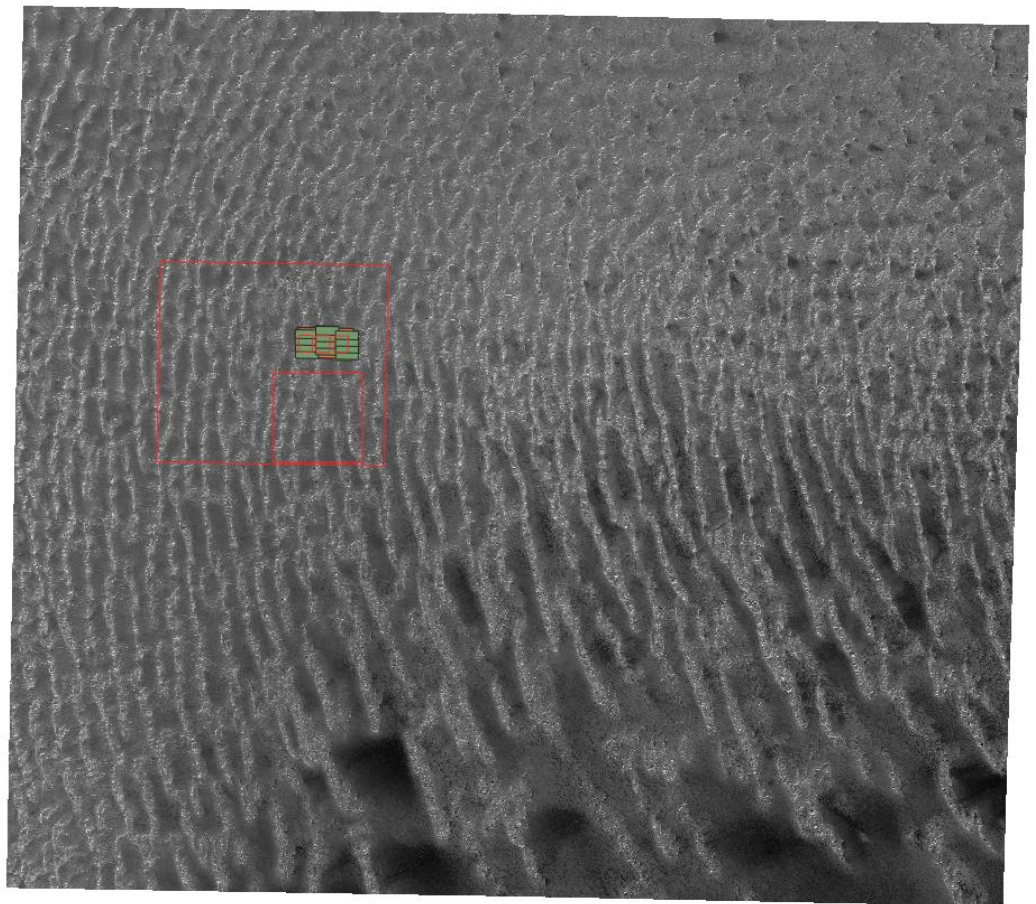


**Figure 4-23: S2A B02 '34RGS' MGRS Tile with the five Libya 4 ROIs (red) and SKS footprints (green).**
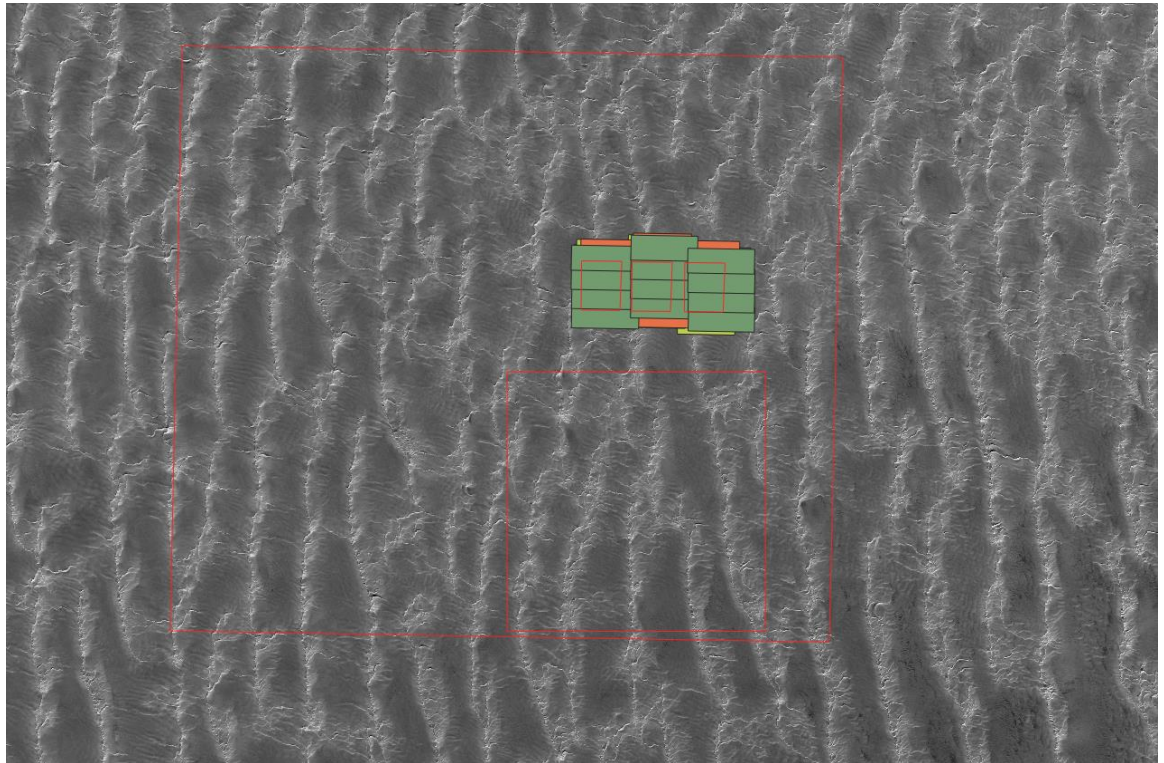
**Figure 4-24: S2A B02 '34RGS' MGRS Tile with the five Libya 4 ROIs (red) and SKS footprints (green), scale 1:100000.**

The following Sentinel 2 MSI products have been used in order to build the calibration reference:

- S2A_MSIL2H_20200108T090341_N9999_R007_T34RGS_20200108T092959.SAFE
- S2A_MSIL2H_20200118T090311_N9999_R007_T34RGS_20200118T092958.SAFE
- S2A_MSIL2H_20200128T090221_N9999_R007_T34RGS_20200128T093015.SAFE
- S2A_MSIL2H_20200207T090131_N9999_R007_T34RGS_20200207T093351.SAFE
- S2A_MSIL2H_20190103T090351_N9999_R007_T34RGS_20190103T110458.SAFE
- S2A_MSIL2H_20190113T090331_N9999_R007_T34RGS_20190113T111955.SAFE
- S2A_MSIL2H_20190123T090251_N9999_R007_T34RGS_20190123T092959.SAFE
- S2A_MSIL2H_20190202T090201_N9999_R007_T34RGS_20190202T093008.SAFE
- S2A_MSIL2H_20190212T090101_N9999_R007_T34RGS_20190212T124529.SAFE
- S2A_MSIL2H_20190222T090001_N9999_R007_T34RGS_20190222T110222.SAFE
- S2A_MSIL2H_20190304T085841_N9999_R007_T34RGS_20190304T101622.SAFE
- S2A_MSIL2H_20190314T085731_N9999_R007_T34RGS_20190314T124056.SAFE
- S2A_MSIL2H_20190324T085621_N9999_R007_T34RGS_20190324T160554.SAFE
- S2A_MSIL2H_20190403T090021_N9999_R007_T34RGS_20190403T113035.SAFE
- S2A_MSIL2H_20190423T085601_N9999_R007_T34RGS_20190423T110404.SAFE
- S2A_MSIL2H_20190503T085601_N9999_R007_T34RGS_20190503T103221.SAFE
- S2A_MSIL2H_20190513T085601_N9999_R007_T34RGS_20190513T110417.SAFE
- S2A_MSIL2H_20190612T085601_N9999_R007_T34RGS_20190612T110225.SAFE
- S2A_MSIL2H_20190622T085601_N9999_R007_T34RGS_20190622T104744.SAFE
- S2A_MSIL2H_20190702T085601_N9999_R007_T34RGS_20190702T112125.SAFE
- S2A_MSIL2H_20190712T085601_N9999_R007_T34RGS_20190712T111856.SAFE
- S2A_MSIL2H_20190722T085601_N9999_R007_T34RGS_20190722T103256.SAFE
- S2A_MSIL2H_20190801T085601_N9999_R007_T34RGS_20190801T112255.SAFE
- S2A_MSIL2H_20190811T085601_N9999_R007_T34RGS_20190811T112400.SAFE

- S2A_MSIL2H_20190821T085601_N9999_R007_T34RGS_20190821T103317.SAFE
- S2A_MSIL2H_20190831T085601_N9999_R007_T34RGS_20190831T111330.SAFE
- S2A_MSIL2H_20190910T085551_N9999_R007_T34RGS_20190910T112242.SAFE
- S2A_MSIL2H_20190920T085631_N9999_R007_T34RGS_20190920T104824.SAFE
- S2A_MSIL2H_20190930T085751_N9999_R007_T34RGS_20190930T110411.SAFE
- S2A_MSIL2H_20191030T090111_N9999_R007_T34RGS_20191030T094817.SAFE
- S2A_MSIL2H_20191109T090201_N9999_R007_T34RGS_20191109T093049.SAFE
- S2A_MSIL2H_20191119T090251_N9999_R007_T34RGS_20191119T093013.SAFE
- S2A_MSIL2H_20191129T090321_N9999_R007_T34RGS_20191129T093130.SAFE
- S2A_MSIL2H_20191219T090401_N9999_R007_T34RGS_20191219T093425.SAFE
- S2A_MSIL2H_20191229T090401_N9999_R007_T34RGS_20191229T093035.SAFE
- S2A_MSIL2H_20200904T085601_N9999_R007_T34RGS_20200904T103841.SAFE
- S2A_MSIL2H_20200914T085601_N9999_R007_T34RGS_20200914T103941.SAFE
- S2A_MSIL2H_20200924T085721_N9999_R007_T34RGS_20200924T111534.SAFE
- S2A_MSIL2H_20200507T085601_N9999_R007_T34RGS_20200507T110432.SAFE
- S2A_MSIL2H_20200527T085601_N9999_R007_T34RGS_20200527T112512.SAFE

For what concern, data observed over La Crau RadCalNet and considered as too bright, products are the following one:

- 20200520_111107_ss01d2_0012_basic_analytic
- 20200525_132031_ssc8d2_0014_basic_analytic
- 20200526_102910_ssc3d2_0014_basic_analytic
- 20200526_131442_ssc10d2_0015_basic_analytic
- 20200622_131156_ssc10d2_0008_basic_analytic
- 20200623_103203_ssc13d2_0014_basic_analytic

## A.3   Anomaly list

The Planet Team report as part of mission / product information a list of known anomalies. These anomalies are listed as follow:

- **Bad pixels** – Planet maintains maps of bad pixels for each sensor and the affected pixels in the images will be filled by interpolating their neighbours.
- Each SKS L1b frame is a composite of up to 30 individual L0 captures. If those individual captures are not well registered, the resulting L1b frame will be blurry[5].
- **Column streaking;** some of the images show streaking effects especially over water or dark areas. These are due to non-linearities in the detector response in the very dark parts of the spectrum
- Problem can occur in the border of the L1b frames in cases there is not enough overlapping coverage
- Problem can occur in the corner of the L1b frames in cases there is not enough overlapping coverage
- For HDR collects over water there are cases with **alternating variations in image** DN (brightness) occurring on the centre detector (detector 2).
- There have been cases, especially under very low sun elevation angles during winter in the Northern Hemisphere, where parts of the values in the analytic (radiance) products all mapped to a minimum value of 1 ( fix on September 14th 2020))
- **Oversharpening** might occur together with saturation and especially blooming
- The most common manifestation of **photo response non-uniformity** in SKS images are repeating 'donut' patterns in the L1b imagery. The donuts can be eliminated by an updated flat field, consisting of gain and offset correction.

---

[5] This has been fixed for PAN images by using phase correlation instead of optical flow for the motion refinement between successive PAN frames. The fix was deployed on October 15th, 2019 RD-5].

- At times, there are noticeable radiometric differences between the detectors within one collect, more precisely between the centre (C2) and the outer cameras (C1 and C3). The root-cause for these radiometric differences is not known
- SKS-A (s1) there is a small area in the red band of CCD 2, where the DNs are constantly too dark
- Since October 28th, 2019 the centre detector of C13 has a flat field problem where it is darker on one side
- Spatial misalignment of individual frames

Product Features:

- Gap and Tears
- Parallax Blurring
- Image Warping
- Block 3Concave footprints: Block 3 satellites C14, C15 and C16 are in a 400 km and not in sun synchronous orbit.
- Movement and Terrain

## A.4 Atmospheric Parameters

Atmospheric parameters (from CAMS Reanalysis data[6]) are used as input of radiative transfer code. Below, values of these parameters are given per date at the time of observation.

**20200905**

Estimate Total colum water vapor: 2.324842419364678

Estimate Ozone content (Dobson) : 0.28134562947098174

Estimate Pression (hpa)          : 1010.5860983809434

Estimate Aot 550 nm          : 0.24577330826478513

**20200911**

Estimate Total colum water vapor: 2.194842857069126

Estimate Ozone content (Dobson) : 0.277872017327908

Estimate Pression (hpa)          : 1008.4106802390193

Estimate Aot 550 nm          : 0.1975588611954936

**20200917**

Estimate Total colum water vapor: 2.402096282885502

Estimate Ozone content (Dobson) : 0.2708464104129835

Estimate Pression (hpa)          : 1013.3158648312315

Estimate Aot 550 nm          : 0.2541982395088862

---

[6] *https://www.ecmwf.int/en/research/climate-reanalysis/cams-reanalysis*

**20200925**

Estimate Total colum water vapor: 2.0660266051810674

Estimate Ozone content (Dobson) : 0.27612188459265075

Estimate Pression (hpa)        : 1013.3356021123112

Estimate Aot 550 nm        : 0.19866922870194617

**20200926**

Estimate Total colum water vapor: 2.341884117569318

Estimate Ozone content (Dobson) : 0.272425221300108

Estimate Pression (hpa)        : 1010.3742265154339

Estimate Aot 550 nm        : 0.1942717268181046

**[END OF DOCUMENT]**